PERGAMON

International Journal of Solids and Structures 40 (2003) 4965–4987

INTERNATIONAL JOURNAL OF SOLIDS and STRUCTURES

www.elsevier.com/locate/ijsolstr

On gravity and centrifugal settling of polydisperse suspensions forming compressible sediments

Stefan Berres, Raimund Bürger *

Institute of Applied Analysis and Numerical Simulation, University of Stuttgart, Pfaffenwaldring 57, D-70569 Stuttgart, Germany

Received 25 August 2002; received in revised form 30 December 2002

Abstract

A mathematical model describing both the hindered settling and the consolidation of suspensions with particles of different sizes and densities forming compressible sediments is presented. The specific new element is a centrifugal configuration, which gives rise to a non-constant body force. Within a range of angular velocities, the model can be reduced to one (radial) space dimension. The result is a system of second-order strongly degenerate parabolic–hyperbolic convection–diffusion equations. For the special subcase of suspensions of rigid spheres, which do not form compressible sediments and for which the effective solid stress can be assumed to vanish, these equations form a first-order system of conservation laws. A type analysis shows that these equations include hyperbolic, hyperbolic–parabolic, and hyperbolic–elliptic systems, depending on the sizes and densities of the solid particles. A numerical high-resolution central difference scheme for the hyperbolic and hyperbolic–parabolic models is applied to solve the model numerically, and thereby to simulate centrifugation of two polydisperse suspensions.

Keywords: Sedimentation; Centrifugation; Polydisperse suspensions; Mathematical model; Simulation

1. Introduction

Mathematical models for the sedimentation and centrifugation of suspensions are important to a variety of applications such as solid–liquid separation in mineral processing and wastewater treatment, classification, fluidization, blood sedimentation and volcanology. In many situations it is necessary to distinguish several particle species, which are assumed to belong to a finite number N of species having sizes $d_1 \geqslant d_2 \geqslant \cdots \geqslant d_N$ and densities $\varrho_1, \ldots, \varrho_N$, where we assume that $d_i \neq d_j$ or $\varrho_i \neq \varrho_j$ for $i \neq j$, $1 \leqslant i, j \leqslant N$. These suspensions are called *polydisperse*, and their characteristic property is particle segregation or differential sedimentation, which results in areas of different composition.

A particularly interesting recent application is provided by a recent series of papers by Biesheuvel and co-workers (Biesheuvel et al., 1998, 2001; Biesheuvel and Verweij, 2000), who show that models for

* Corresponding author. Tel.: +49-711-6857647; fax: +49-711-6855599.
E-mail addresses: berres@mathematik.uni-stuttgart.de (S. Berres), buerger@mathematik.uni-stuttgart.de (R. Bürger).

0020-7683/$ - see front matter © 2003 Elsevier Ltd. All rights reserved.
doi:10.1016/S0020-7683(03)00249-X

polydisperse sedimentation covering the full range from dilute suspensions to concentrated sediments are useful in models of manufacturing of solid products (casts) formed of small particles. In this paper, we develop, in part analyze, and simulate models which indeed cover the full range of concentrations.

In the sequel, the present paper is outlined and put in the proper perspective of the literature. In Section 2 we derive a mathematical model for the separation of polydisperse suspensions of rigid spheres under both a centrifugal and a gravitational body force. The local composition of such a mixture is described by the vector $\Phi := (\phi_1, \ldots, \phi_N)^{\mathrm{T}}$ of concentrations, where ϕ_i is the local volume concentration of particle species i, $i = 1, \ldots, N$, having size d_i and density ϱ_i. The modeling starts from the usual mass and linear momentum balance equations for the N solids species (each regarded as one phase) and the fluid. The material properties of the suspension are introduced by constitutive assumptions on the solid and fluid stress tensors and the solid–fluid interaction forces. In particular, the solid and fluid phase pressures are expressed in terms of the effective solid stress σ_e and the pore pressure. Specifying the solid–fluid interaction force for each species and finally performing a dimensional analysis, which permits neglecting several terms from the linear momentum balance equations, we obtain the solid–fluid relative velocity (or slip velocity) of each species as a function of Φ and $\nabla\Phi$, which yields the fluxes of the continuity equations. The final (spatially multidimensional) model equations form a strongly degenerate system of N convection–diffusion equations for $\phi_1, \ldots, \phi_N$ coupled to the divergence-free condition of the volume-average mixture velocity and a three-component equation for the motion of the mixture.

The multidimensional model is further restricted to one space dimension. In this case, the mixture velocity is zero for settling in a closed vessel. Wall effects may be neglected since the particles are small against the vessel diameter. For a centrifugal system, the reduction to one space dimension is admissible only if both the gravitational body force and the Coriolis force, introducing an azimuthal velocity component, are negligible. We consider either a rotating tube (Fig. 1(a)) or a basket centrifuge (Fig. 1(b)), and distinguish between these cases by a parameter σ taking the values zero and one in the tube and basket cases, respectively.

Under these simplifications, only a system of N second-order strongly degenerate convection–diffusion equations for the N solids concentrations $\phi_1, \ldots, \phi_N$ as functions of height z or radius r and time t have to be solved if sediment compressibility is taken into account, and these equations further reduce to a first-order system of conservation laws in the absence of compressibility, that is, when the particles are rigid spheres. These equations are equipped with an initial concentration distribution and boundary conditions to form a solvable mathematical model. Since the result of our derivation is similar to models proposed by Masliyah (1979) and Lockett and Bassoon (1979), we refer to these equations as the MLB model, as opposed for example to the Davis and Gecol (1994) or Patwardhan and Tien (1985) models.

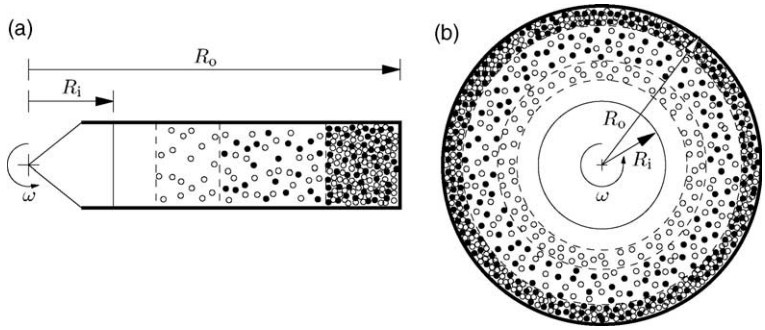

Fig. 1. Centrifugal separation of a bidisperse suspension of light (○) and heavy (●) particles (a) in a rotating tube ($\sigma = 0$) and (b) in a basket centrifuge ($\sigma = 1$).

The resulting spatially one-dimensional systems of convection–diffusion equations have some interesting mathematical properties. It is not trivial to determine the type of these equations in dependence of the number of species N, their sizes and densities, and the local concentration vector Φ. The basic results for the MLB model are summarized in Section 3. It turns out that the MLB model is in general non-hyperbolic or (for $N = 2$) hyperbolic–elliptic, that is, of mixed type for suspensions with particles of different densities, but according to Berres et al. (2003a) it is always hyperbolic for suspensions of equal-density spheres with arbitrary size distributions. Only in the hyperbolic case it is ensured that all solution information travels at finite speed. The condition for loss of hyperbolicity is equivalent to an instability condition predicting the occurrence of horizontal structures like 'fingers', 'blobs' and 'columns' during the separation of a polydisperse suspension. This instability condition was first derived by Batchelor and Janse van Rensburg (1986) for $N = 2$ and recently extended to arbitrary N, and identified as a condition for the system to be of mixed type, by Bürger et al. (2000b, 2002). Such mixed systems appear in many applications (Fitt, 1996), but the interesting point in ours is that such 'fingers', 'blobs' and 'columns' have indeed been observed and that predictions of their occurrence by means of Batchelor and Janse van Rensburg's criterion are fairly accurate. The strict hyperbolicity result by Berres et al. (2003a) is consistent with the lack of any observation of instability phenomena for equal-density particles.

We employ the high-resolution central difference scheme by Kurganov and Tadmor (2000) to simulate centrifugal separation of polydisperse suspensions with compression. For additional material on these schemes we refer to Tadmor (1998). A full description of the scheme in the application to polydisperse gravity sedimentation of ideal suspensions consisting of rigid spheres, which is described by first-order systems of conservation laws, is given by Bürger et al. (2001). The Kurganov–Tadmor scheme is a refinement of the essentially non-oscillatory central difference scheme by Nessyahu and Tadmor (1990) used in Bürger et al. (2000a). Kurganov and Tadmor (2000) also propose an extension of their scheme to strongly degenerate parabolic–hyperbolic systems. The application of that extension to the 'gravity' initial-boundary value problem formulated in Section 2 is described in full detail by Berres et al. (2003a). Only some minor modifications are needed in order to make that scheme work also for the 'centrifugal' initial-boundary value problem. For sake of brevity, we state in Section 4 only those steps of the scheme that differ from the description by Berres et al. (2003a).

Section 5 illustrates the mathematical model by numerical simulations. Simulations of gravity sedimentation of polydisperse suspensions of rigid spheres (not forming compressible sediments) based on numerical solution of a first-order system have been presented by several authors (Lee, 1989; Concha et al., 1992; Zeng and Lowe, 1992; Flotats, 1995; Bürger et al., 2000a, 2001; Berres et al., 2003b; Xue and Sun, 2003). The effect of compressible sediment for polydisperse gravity settling has been considered by Shih et al. (1986), Stamatakis and Tien (1992) and Berres et al. (2003a). In view of all these published results and since our novel contribution is the extension of the polydisperse sedimentation model to centrifugal configurations, the simulations presented in Section 5 are limited to the centrifugal case.

A brief concluding discussion of the model is given in Section 6.

2. Derivation of the mathematical model

2.1. Mass and linear momentum balances

The local mass balance equations of the solid species and of the fluid can be written as

$$\frac{\partial \phi_i}{\partial t} + \nabla \cdot (\phi_i \mathbf{v}_i) = 0, \quad i = 1, \ldots, N, \tag{2.1}$$

$$-\frac{\partial \phi}{\partial t} + \nabla \cdot ((1-\phi)\mathbf{v}_\mathrm{f}) = 0, \tag{2.2}$$

where $\mathbf{v}_1, \ldots, \mathbf{v}_N$ and $\mathbf{v}_\mathrm{f}$ are the phase velocities of the solid species and the fluid, respectively, and $\phi = \phi_1 + \cdots + \phi_N$ is the total volumetric solids concentration. Defining the volume-average velocity of the mixture $\mathbf{q} := (1-\phi)\mathbf{v}_\mathrm{f} + \phi_1\mathbf{v}_1 + \cdots + \phi_N\mathbf{v}_N$ and the relative velocities or slip velocities $\mathbf{u}_i := \mathbf{v}_i - \mathbf{v}_\mathrm{f}$ for $i = 1, \ldots, N$, we obtain

$$\phi_i \mathbf{v}_i = \phi_i(\mathbf{u}_i + \mathbf{q} - (\phi_1\mathbf{u}_1 + \cdots + \phi_N\mathbf{u}_N)), \quad i = 1, \ldots, N, \tag{2.3}$$

such that Eq. (2.1) can be rewritten in terms of $\mathbf{q}$ and $\mathbf{u}_1, \ldots, \mathbf{u}_N$ as

$$\frac{\partial \phi_i}{\partial t} + \nabla \cdot (\phi_i\mathbf{u}_i + \phi_i\mathbf{q} - \phi_i(\phi_1\mathbf{u}_1 + \cdots + \phi_N\mathbf{u}_N)) = 0, \quad i = 1, \ldots, N. \tag{2.4}$$

The sum of all equations in (2.1) and (2.2) produces the simple mass balance of the mixture,

$$\nabla \cdot \mathbf{q} = 0. \tag{2.5}$$

The momentum balance equations for the N solid species and the fluid are

$$\varrho_i \phi_i \frac{\mathrm{D}\mathbf{v}_i}{\mathrm{D}t} = \nabla \cdot \mathbf{T}_i + \varrho_i \phi_i \mathbf{b}_i + \mathbf{m}_i^\mathrm{f} + \mathbf{m}_i^\mathrm{s}, \quad i = 1, \ldots, N, \tag{2.6}$$

$$\varrho_\mathrm{f}(1-\phi)\frac{\mathrm{D}\mathbf{v}_\mathrm{f}}{\mathrm{D}t} = \nabla \cdot \mathbf{T}_\mathrm{f} + \varrho_\mathrm{f}(1-\phi)\mathbf{b}_\mathrm{f} - (\mathbf{m}_1^\mathrm{f} + \cdots + \mathbf{m}_N^\mathrm{f}). \tag{2.7}$$

Here ϱ_f is the mass density of the fluid, $\mathbf{T}_i$ denotes the stress tensor of particle species i, $i = 1, \ldots, N$, $\mathbf{T}_\mathrm{f}$ that of the fluid, $\mathbf{b}_i$ and $\mathbf{b}_\mathrm{f}$ are the body forces acting on solids species i and on the fluid, respectively, $\mathbf{m}_i^\mathrm{f}$ and $\mathbf{m}_{ij}^\mathrm{s}$ are the interaction forces per unit volume between solid species i and the fluid and between the solid species i and j, respectively, $\mathbf{m}_i^\mathrm{s} := \mathbf{m}_{i1}^\mathrm{s} + \cdots + \mathbf{m}_{iN}^\mathrm{s}$ is the particle–particle interaction term of species i, and we use the standard notation $\mathrm{D}\mathbf{v}/\mathrm{D}t := \partial\mathbf{v}/\partial t + (\mathbf{v} \cdot \nabla)\mathbf{v}$.

2.2. Solid and fluid stress tensors

We assume that the stress tensors of the solid and fluid phases take the respective forms $\mathbf{T}_i = -p_i\mathbf{I} + \mathbf{T}_i^\mathrm{E}$ for $i = 1, \ldots, N$ and $\mathbf{T}_\mathrm{f} = -p_\mathrm{f}\mathbf{I} + \mathbf{T}_\mathrm{f}^\mathrm{E}$, where p_i denotes the phase pressure of particle species i, p_f that of the fluid, $\mathbf{I}$ denotes the identity tensor, and $\mathbf{T}_i^\mathrm{E}$ and $\mathbf{T}_\mathrm{f}^\mathrm{E}$ are the extra (or viscous) stress tensors of particle species i and the fluid, respectively. However, viscous effects due to the motion of the mixture are not considered to be dominant and we therefore assign all viscous effects to the fluid extra stress tensor. Thus, we assume that ν_0^f and $\nu_0^\mathrm{s} < \nu_0^\mathrm{f}$ are characteristic viscosities associated with the fluid and the solid species, respectively. These quantities are introduced here to provide justification for neglecting the viscous stress tensors as a consequence of the dimensional analysis.

2.3. Partial pressures, pore pressures and effective solids stress

The phase pressures $p_1, \ldots, p_N$ and p_f are theoretical variables, which cannot be measured experimentally. As in the studies by Concha et al. (1996), Berres et al. (2003a) and Bürger et al. (2000b, 2002), they are expressed in terms of the pore pressure p and the effective solids stress σ_e, which can be measured and therefore are experimental variables. In the monodisperse case, σ_e is given by a constitutive equation of the type $\sigma_\mathrm{e} = \sigma_\mathrm{e}(\phi)$. We could assume here that σ_e is given as a function of the local composition of the mixture, $\sigma_\mathrm{e} = \sigma_\mathrm{e}(\Phi)$. However, as noted by Stamatakis and Tien (1992), no suitable general relationship of this type for polydisperse suspensions has been derived theoretically or empirically so far. Instead, we

follow existing studies (Shih et al., 1986; Massoudi et al., 1992; Stamatakis and Tien, 1992) and express σ_e, as in the monodisperse case, simply as a function of the local porosity $\varepsilon = 1 - (\phi_1 + \cdots + \phi_N) = 1 - \phi$ or equivalently, of the cumulative solids concentration ϕ only. The generic assumptions on σ_e are

$$\sigma_e(\phi)\begin{cases} = 0 & \text{for } \phi \leqslant \phi_c, \\ > 0 & \text{for } \phi > \phi_c, \end{cases} \quad \sigma_e'(\phi) := \frac{d\sigma_e(\phi)}{d\phi}\begin{cases} = 0 & \text{for } \phi \leqslant \phi_c, \\ > 0 & \text{for } \phi > \phi_c, \end{cases} \tag{2.8}$$

where ϕ_c is the critical concentration at which the solid particles touch each other. Very frequently the following power law equation is used (Tiller and Leu, 1980):

$$\sigma_e(\phi) = \begin{cases} 0 & \text{for } \phi \leqslant \phi_c, \\ \sigma_0((\phi/\phi_c)^k - 1) & \text{for } \phi > \phi_c. \end{cases} \tag{2.9}$$

The relationship between the theoretical pressures $p_1, \ldots, p_N$ and p_f and the experimental variables p and $\sigma_e(\phi)$ is established in full detail by Berres et al. (2003a). We briefly sketch the main arguments here.

The pore pressure p is defined within the fluid filling the interstices of the solids, while the partial fluid pressure p_f is defined in the fluid component occupying the whole volume of the mixture. This assumption leads to the equation $p_f = (1 - \phi)p$. Moreover, the total stress of the mixture p_t can be written in two different ways as $p_t = p_1 + \cdots + p_N + p_f = p + \sigma_e(\phi)$. We assume that for each solids species its surface cross-sectional area fraction equals its local volume fraction ϕ_i (a formal justification for this assumption is given by Bürger et al., 2002). This suggests relating $p_1, \ldots, p_N$ to p and $\sigma_e(\phi)$ by

$$p_i = \frac{\phi_i}{\phi}(\phi p + \sigma_e(\phi)), \quad i = 1, \ldots, N. \tag{2.10}$$

2.4. Body force, solid–fluid and particle–particle interaction forces

So far the derivation of the model equations has followed that of the gravitational sedimentation–consolidation model by Berres et al. (2003a). We here extend this model to centrifugation by assuming that the body forces $\mathbf{b}_1, \ldots, \mathbf{b}_N$ and $\mathbf{b}_f$ take the respective forms

$$\mathbf{b}_i = -g\mathbf{k} - \boldsymbol{\omega} \times \boldsymbol{\omega} \times \mathbf{r} - 2\boldsymbol{\omega} \times \mathbf{v}_i, \quad i = 1, \ldots, N, \tag{2.11}$$

$$\mathbf{b}_f = -g\mathbf{k} - \boldsymbol{\omega} \times \boldsymbol{\omega} \times \mathbf{r} - 2\boldsymbol{\omega} \times \mathbf{v}_f, \tag{2.12}$$

where $\boldsymbol{\omega} = \omega\mathbf{c}$ is the angular velocity of the rotating system, ω is the angular speed, $\mathbf{c}$ (with $\|\mathbf{c}\| = 1$) is the unit vector of its axis of rotation and $\mathbf{r}$ is the radius vector of the system. In each of Eqs. (2.11) and (2.12), the first term denotes the gravitational force and the second and third term represent the inertial forces originating from the centripetal and Coriolis forces, which are both product of the moving frame of reference. The body forces $\mathbf{b}_1, \ldots, \mathbf{b}_N$ and $\mathbf{b}_f$ can be decomposed into two parts, a conservative force $\nabla(\Psi + \Omega)$ with the potentials $\Psi := -\mathbf{g} \cdot \mathbf{r} = -g\mathbf{k} \cdot \mathbf{r} \equiv g \cdot z$ and $\Omega := -(1/2)(\boldsymbol{\omega} \times \mathbf{r}) \cdot (\boldsymbol{\omega} \times \mathbf{r}) = -(1/2)\omega^2 r^2$, and the non-conservative parts $-2\boldsymbol{\omega} \times \mathbf{v}_i$, $i = 1, \ldots, N$ and $-2\boldsymbol{\omega} \times \mathbf{v}_f$, so that $\mathbf{b}_1, \ldots, \mathbf{b}_N$ and $\mathbf{b}_f$ can be written as $\mathbf{b}_i = -\nabla(\Psi + \Omega) - 2\boldsymbol{\omega} \times \mathbf{v}_i$ for $i = 1, \ldots, N$ and $\mathbf{b}_f = -\nabla(\Psi + \Omega) - 2\boldsymbol{\omega} \times \mathbf{v}_f$.

The ratio between the representative centrifugal and gravity components of $\mathbf{b}_1, \ldots, \mathbf{b}_N$ and $\mathbf{b}_f$ is expressed by the Froude number of the system (not of the flow) defined by $\mathscr{F} := \omega^2 R/g$, where R is a typical distance to the axis of rotation (for example, the outer radius of the container). We are here mainly interested in the limiting cases $\mathscr{F} = 0$ (gravity settling) and $\mathscr{F} = \infty$ (for a centrifugally dominated configuration).

The interaction force between the different solid particle species described by the term $\mathbf{m}_i^s = \mathbf{m}_{i1}^s + \cdots + \mathbf{m}_{iN}^s$ could be specified by the formula due to Nakamura and Capes (1976):

$$\mathbf{m}_{ij}^{\mathrm{s}} = \frac{3}{2}\varphi_{\mathrm{e}}\frac{\varrho_i\varrho_j\phi_i\phi_j(d_i+d_j)^2}{\varrho_i d_i^3+\varrho_j d_j^3}\left\|\mathbf{v}_i-\mathbf{v}_j\right\|(\mathbf{v}_i-\mathbf{v}_j),\quad i,j=1,\ldots,N,\ i\neq j,$$

where the parameter φ_{e} accounts for non-head-on-collisions (Shih et al., 1986) and its value depends on whether these are plastic or elastic. Typical values of φ_{e} vary between zero and five (Nakamura and Capes, 1976; Arastoopour et al., 1982), and numerical simulations have not turned out to be sensitive to φ_{e}. However, there is experimental and theoretical evidence that $\mathbf{m}_i^{\mathrm{s}}$ can be neglected at the very low Reynolds numbers considered here, see Bürger et al. (2002) for details. As in previous papers, we assume that the solid–fluid interaction term $\mathbf{m}_i^{\mathrm{f}}$ corresponding to species i is given by $\mathbf{m}_i^{\mathrm{f}} = \alpha_i(\Phi)\mathbf{u}_i + \beta\nabla\phi_i$ for $i=1,\ldots,N$, where $\alpha_i(\Phi)$ denotes the resistance coefficient related to the transfer of momentum between the fluid and particle species i. Considering the system at equilibrium, that is assuming $\mathbf{v}_{\mathrm{f}}=0$, $\mathbf{v}_1=\cdots=\mathbf{v}_N=0$, and that the pore pressure equals the hydrostatic pressure, i.e. $\nabla p = \varrho_{\mathrm{f}}(-g\mathbf{k}+(\omega^2/2)\mathbf{r})$, we may conclude that $\beta = p$.

Inserting all assumptions into the linear momentum balance equations (2.6) and (2.7), we obtain the balance equations

$$\begin{aligned}\varrho_i\phi_i\frac{\mathrm{D}\mathbf{v}_i}{\mathrm{D}t} &= \varrho_i\phi_i(-g\mathbf{k}+\omega^2\mathbf{r}) - 2\varrho_i\phi_i\omega\mathbf{c}\times\mathbf{v}_i + \nabla\cdot\mathbf{T}_{\mathrm{f}}^{\mathrm{E}} - \phi_i\nabla p + \alpha_i(\Phi)\mathbf{u}_i + \mathbf{m}_i^{\mathrm{s}}\\ &\quad - \nabla\left(\frac{\phi_i}{\phi}\sigma_{\mathrm{e}}(\phi)\right),\quad i=1,\ldots,N,\end{aligned} \tag{2.13}$$

$$\nabla p = \varrho_{\mathrm{f}}(-g\mathbf{k}+\omega^2\mathbf{r}) - 2\varrho_{\mathrm{f}}\omega\mathbf{c}\times\mathbf{v}_{\mathrm{f}} - \frac{1}{1-\phi}(\alpha_1(\Phi)\mathbf{u}_1+\cdots+\alpha_N(\Phi)\mathbf{u}_N) - \varrho_{\mathrm{f}}\frac{\mathrm{D}\mathbf{v}_{\mathrm{f}}}{\mathrm{D}t} + \frac{1}{1-\phi}\nabla\cdot\mathbf{T}_{\mathrm{f}}^{\mathrm{E}}. \tag{2.14}$$

2.5. Dimensional analysis

Considerable simplification of the linear momentum balance equations (2.13) and (2.14) can be achieved by an order-of-magnitude study or dimensional analysis. We assume that characteristic quantities of our system are a typical length L_0, a representative particle size d, a typical velocity U_0, a reference scalar angular velocity ω_0 and a kinematic viscosity ν_0. Moreover, we refer all densities to that of the fluid, ϱ_{f}, and choose $t_0 = L_0/U_0$ as a time scale for dimensionless time derivatives. Introducing the characteristic parameters into (2.13) and (2.14) and defining the Froude number of the flow, $\mathsf{Fr} := U_0^2/(gL_0)$, the Rossby number $\mathsf{Ro} := U_0/(\omega_0 L_0)$ and the sedimentation Reynolds number $\mathsf{Re} := U_0L_0/\nu_0$, we get the following equations in terms of the dimensionless variables, where a star denotes the dimensionless version of each previously introduced quantity:

$$\begin{aligned}\varrho_i^*\phi_i\mathsf{Fr}\frac{\mathrm{D}\mathbf{v}_i^*}{\mathrm{D}t^*} &= \varrho_i^*\phi_i(-\mathbf{k}+\mathscr{F}(\omega^*)^2\mathbf{r}^*) - 2\varrho_i^*\phi_i\frac{\mathsf{Fr}}{\mathsf{Ro}}\omega^*\mathbf{c}\times\mathbf{v}_i^* + \frac{d}{L_0}\frac{v_0^{\mathrm{s}}}{v_0^{\mathrm{f}}}\frac{\mathsf{Fr}}{\mathsf{Re}}\nabla^*\cdot(\mathbf{T}_{\mathrm{f}}^{\mathrm{E}})^* - \phi_i\nabla^*p^*\\ &\quad + \alpha_i^*(\Phi)\mathbf{u}_i^* + \frac{L}{d}\mathsf{Fr}(\mathbf{m}_i^{\mathrm{s}})^* - \nabla^*\left(\frac{\phi_i}{\phi}\sigma_{\mathrm{e}}^*(\phi)\right),\quad i=1,\ldots,N,\end{aligned} \tag{2.15}$$

$$\begin{aligned}\nabla^*p^* &= -\mathbf{k}+\mathscr{F}(\omega^*)^2\mathbf{r}^* - 2\frac{\mathsf{Fr}}{\mathsf{Ro}}\omega^*\mathbf{c}\times\mathbf{v}_{\mathrm{f}}^* - \frac{1}{1-\phi}(\alpha_1^*(\Phi)\mathbf{u}_1^*+\cdots+\alpha_N^*(\Phi)u_N^*) - \mathsf{Fr}\frac{\mathrm{D}\mathbf{v}_{\mathrm{f}}^*}{\mathrm{D}t^*}\\ &\quad + \frac{1}{1-\phi}\frac{d}{L}\frac{\mathsf{Fr}}{\mathsf{Re}}\nabla^*\cdot(\mathbf{T}_{\mathrm{f}}^{\mathrm{E}})^*.\end{aligned} \tag{2.16}$$

Typical values of the constants involved are $g = 10$ m/s^2 (acceleration of gravity), $L_0 = 0.1$ m (sedimentation space in a centrifuge), $U_0 = 10^{-4}$ m/s (assumed settling velocity of the largest particle in unbounded, quiescent fluid) and $\nu_0 = 10^{-6}$ m^2/s (kinematic viscosity of water). These values imply $\mathsf{Fr} = 10^{-8}$ and $\mathsf{Fr}/\mathsf{Re} = 10^{-7}$. The value of ω_0 and thus those of $\mathscr{F}$ and Ro will be specified later.

On the basis of these values and the standard assumption that the starred terms are of the order of magnitude $\mathcal{O}(1)$, we may neglect the viscous and convective acceleration terms in the linear momentum balances, which bear the coefficients Fr and Fr/Re. For reasons to be discussed later, the viscous term in the linear momentum balance of the fluid will be retained.

In view of the kinematic relationships $\mathbf{v}_i = \mathbf{u}_i + \mathbf{q} - (\phi_1\mathbf{u}_1 + \cdots + \phi_N\mathbf{u}_N)$ for $i = 1, \ldots, N$ and $\mathbf{v}_\mathrm{f} = \mathbf{q} - (\phi_1\mathbf{u}_1 + \cdots + \phi_N\mathbf{u}_N)$, which follow from the definitions of the slip velocities and of $\mathbf{q}$, the reduced non-dimensional linear momentum balance equations can be written as

$$\begin{aligned}\alpha_i^*(\Phi)\mathbf{u}_i^* = {} & \varrho_i^*\phi_i(\mathbf{k} - \mathscr{F}(\omega^*)^2\mathbf{r}^*) + 2\varrho_i^*\phi_i\frac{\mathsf{Fr}}{\mathsf{Ro}}\omega^*\mathbf{c}\times(\mathbf{u}_i^* + \mathbf{q}^* - (\phi_1\mathbf{u}_1^* + \cdots + \phi_N\mathbf{u}_N^*)) \\ & + \nabla^*\left(\frac{\phi_i}{\phi}\sigma_\mathrm{e}^*(\phi)\right) + \phi_i\nabla p^*, \quad i = 1, \ldots, N,\end{aligned} \tag{2.17}$$

$$\begin{aligned}\nabla^* p^* = {} & -\mathbf{k} + \mathscr{F}(\omega^*)^2 - \frac{1}{1-\phi}(\alpha_1^*(\Phi)\mathbf{u}_1^* + \cdots + \alpha_N^*(\Phi)\mathbf{u}_N^*) + \frac{1}{1-\phi}\frac{d}{L}\frac{\mathsf{Fr}}{\mathsf{Re}}\nabla^*\cdot(\mathbf{T}_\mathrm{f}^\mathrm{E})^* \\ & - 2\frac{\mathsf{Fr}}{\mathsf{Ro}}\omega^*\mathbf{c}\times(\mathbf{q} - (\phi_1\mathbf{u}_1^* + \cdots + \phi_N\mathbf{u}_N^*)).\end{aligned} \tag{2.18}$$

Inserting (2.18) into each of Eqs. (2.17) and discarding the unique small term according to the previous considerations, namely the viscous term, we obtain after simplifications

$$\begin{aligned}\alpha_i^*(\Phi)\mathbf{u}_i^* = {} & \phi_i(\varrho_i^* - 1)(\mathbf{k} - \mathscr{F}(\omega^*)^2\mathbf{r}^*) + 2\phi_i\frac{\mathsf{Fr}}{\mathsf{Ro}}\omega^*\mathbf{c}\times\mathbf{u}_i^* + \nabla^*\left(\frac{\phi_i}{\phi}\sigma_\mathrm{e}^*(\phi)\right) \\ & - \frac{\phi_i}{1-\phi}(\alpha_1^*(\Phi)\mathbf{u}_1^* + \cdots + \alpha_N^*(\Phi)\mathbf{u}_N^*), \quad i = 1, \ldots, N.\end{aligned} \tag{2.19}$$

We are now interested in those limiting cases for which (2.19) produces an easily solvable linear system for the slip velocities $\mathbf{u}_1^*, \ldots, \mathbf{u}_N^*$. One simple case occurs when $\omega = 0$ and thus $\mathscr{F} = 0$, which corresponds to the gravity settling model studied by Berres et al. (2003a). On the other hand, if we wish to include centrifugation, then for moderate angular velocities the ratio Fr/Ro still remains small and admits neglecting the Coriolis terms. For example, consider the range 100 rad/s $\leqslant \omega_0 \leqslant$ 1000 rad/s, which corresponds to about 1000–10 000 rpm, and $R = L_0 = 0.1$ m. We then have $\mathsf{Fr}/\mathsf{Ro} = 10^{-5}$ and $\mathscr{F} = 100$ for $\omega_0 = 100$ rad/s and $\mathsf{Fr}/\mathsf{Ro} = 10^{-4}$ and $\mathscr{F} = 10\,000$ for $\omega_0 = 10\,000$ rad/s. This illustrates that neglecting both gravity and Coriolis terms still produces a reasonable approximation for a centrifugal system within a certain range of angular velocities. We thus assume that Fr/Ro is small and delete the corresponding terms from (2.19). Switching back to dimensional variables, we obtain

$$\alpha_i(\Phi)\mathbf{u}_i + \frac{\phi_i}{1-\phi}(\alpha_1(\Phi)\mathbf{u}_1 + \cdots + \alpha_N(\Phi)\mathbf{u}_N) = \mathbf{c}_i, \tag{2.20}$$

$$\mathbf{c}_i := \phi_i(\varrho_i - \varrho_\mathrm{f})(g\mathbf{k} - \omega^2\mathbf{r}) + \nabla\left(\frac{\phi_i}{\phi}\sigma_\mathrm{e}(\phi)\right), \quad i = 1, \ldots, N.$$

This linear system of equations for $\mathbf{u}_1, \ldots, \mathbf{u}_N$ can be solved explicitly by the Sherman–Morrison formula, which states that for a matrix $\mathbf{B}$ of the type $\mathbf{B} = \mathbf{D} + \mathbf{x}\mathbf{y}^\mathrm{T}$, where $\mathbf{D}$ is an invertible diagonal matrix and $\mathbf{x}$ and $\mathbf{y}$ are given vectors, its inverse $\mathbf{B}^{-1}$ is given by

$$\mathbf{B}^{-1} = (\mathbf{D} + \mathbf{x}\mathbf{y}^{\mathrm{T}})^{-1} = \mathbf{D}^{-1} - \frac{1}{1 + \mathbf{y}^{\mathrm{T}}\mathbf{D}^{-1}\mathbf{x}}\mathbf{D}^{-1}\mathbf{x}\mathbf{y}^{\mathrm{T}}\mathbf{D}^{-1}.$$

In our case, we get the following solution of the system (2.20):

$$\mathbf{u}_i = \frac{\phi_i}{\alpha_i(\Phi)(1-\phi)}(\mathbf{c}_i - (\phi_1\mathbf{c}_1 + \cdots + \phi_N\mathbf{c}_N)), \quad i = 1, \ldots, N. \tag{2.21}$$

We consider here the Masliyah–Lockett–Bassoon model (MLB) (Masliyah, 1979; Lockett and Bassoon, 1979), whose decisive specific assumption states that there exists a function $V(\phi)$, the 'hindered settling factor', such that $\phi_i/\alpha_i(\Phi) = -d_i^2 V(\phi)/(18\mu_{\mathrm{f}})$ for $i = 1, \ldots, N$, where μ_{f} is the dynamic viscosity of the pure fluid. A very common example due to Richardson and Zaki (1954) is

$$V(\phi) = \begin{cases} (1-\phi)^{n-2}, & n > 2 \quad \text{for } 0 < \phi < 1, \\ 0 & \text{otherwise.} \end{cases} \tag{2.22}$$

Introducing the reduced densities $\bar{\varrho}_i := \varrho_i - \varrho_{\mathrm{s}}$, $i = 1, \ldots, N$, the vector $\bar{\boldsymbol{\varrho}} := (\bar{\varrho}_1, \ldots, \bar{\varrho}_N)^{\mathrm{T}}$ and the parameters $\mu := -gd_1^2/(18\mu_{\mathrm{f}})$ and $\delta_i := d_i^2/d_1^2$ for $i = 1, \ldots, N$, we finally obtain the explicit equations for the slip velocities

$$\mathbf{u}_i = \mu\delta_i V(\phi)\left[(\bar{\varrho}_i - \bar{\boldsymbol{\varrho}}^{\mathrm{T}}\Phi)\left(\mathbf{k} - \frac{\omega^2}{g}\mathbf{r}\right) + \frac{\sigma_{\mathrm{e}}(\phi)}{\phi_i}\nabla\left(\frac{\phi_i}{\phi}\right) + \frac{1-\phi}{\phi}\nabla\sigma_{\mathrm{e}}(\phi)\right], \quad i = 1, \ldots, N. \tag{2.23}$$

In view of (2.3), the fluxes $\phi_1\mathbf{v}_1, \ldots, \phi_N\mathbf{v}_N$ appearing in the solids continuity equations can be written as

$$\phi_i\mathbf{v}_i = f_i^{\mathrm{M}}(\Phi)\left(\mathbf{k} - \frac{\omega^2}{g}\mathbf{r}\right) + \phi_i\mathbf{q} - \mathbf{a}_i(\Phi, \nabla\Phi), \quad i = 1, \ldots, N, \tag{2.24}$$

where, defining $\boldsymbol{\delta} := (\delta_1, \ldots, \delta_N)^{\mathrm{T}}$, we have

$$f_i^{\mathrm{M}}(\Phi) := \mu V(\phi)\phi_i\left[\delta_i(\bar{\varrho}_i - \bar{\boldsymbol{\varrho}}^{\mathrm{T}}\Phi) - \sum_{k=1}^{N}\delta_k\phi_k(\bar{\varrho}_k - \bar{\boldsymbol{\varrho}}^{\mathrm{T}}\Phi)\right], \tag{2.25}$$

$$\mathbf{a}_i(\Phi, \nabla\Phi) := -\frac{\mu V(\phi)}{g}\left[\frac{(1-\phi)\phi_i}{\phi}(\delta_i - \boldsymbol{\delta}^{\mathrm{T}}\Phi)\nabla\sigma_{\mathrm{e}}(\phi) + \sigma_{\mathrm{e}}(\phi)\left(\delta_i\nabla\left(\frac{\phi_i}{\phi}\right) - \phi_i\sum_{k=1}^{N}\delta_k\nabla\left(\frac{\phi_k}{\phi}\right)\right)\right], \quad i = 1, \ldots, N. \tag{2.26}$$

Thus, the field equations that have to be solved in several space dimensions are

$$\frac{\partial\phi_i}{\partial t} + \nabla\cdot\left\{\phi_i\mathbf{q} + f_i^{\mathrm{M}}(\Phi)\left(\mathbf{k} - \frac{\omega^2}{g}\mathbf{r}\right)\right\} = \nabla\cdot\mathbf{a}_i(\Phi, \nabla\Phi), \quad i = 1, \ldots, N, \tag{2.27}$$

$$\nabla\cdot\mathbf{q} = 0, \tag{2.28}$$

$$\nabla p = -\nabla\sigma_{\mathrm{e}}(\phi) + \varrho(\Phi)(-g\mathbf{k} + \omega^2\mathbf{r}) + \frac{1}{1-\phi}\nabla\cdot\mathbf{T}_{\mathrm{f}}^{\mathrm{E}}. \tag{2.29}$$

We are interested in simple spatially one-dimensional cases in which only the system of convection–diffusion equation (2.27) rather than the full coupled system (2.27)–(2.29) has to be solved. The obvious cases are gravity settling in a closed column and batch centrifugation in a tube or basket centrifuge neglecting the effect of gravity. This case has been studied only for monodisperse flocculated suspensions so far (Bürger and Concha, 2001).

2.6. Gravity settling in a closed column

We set $\omega = 0$ and assume that all variables depend on height z, taken in the positive direction of the vector $\mathbf{k}$ only. Then (2.28) turns into $\partial q/\partial z = 0$ and thus $q = 0$ in view of the closed bottom boundary condition. The only system that remains to be solved can be written as

$$\frac{\partial \Phi}{\partial t} + \frac{\partial \mathbf{f}^{\mathrm{M}}(\Phi)}{\partial z} = \frac{\partial}{\partial z}\left(\mathbf{A}(\Phi)\frac{\partial \Phi}{\partial z}\right), \tag{2.30}$$

where the entries of the diffusion matrix $\mathbf{A}(\Phi) = (\eta_{ij}(\Phi))_{1\leqslant i,j\leqslant N}$ are given by

$$\eta_{ij}(\Phi) := -\frac{\mu V(\phi)}{g\phi}\left\{(1-\phi)\phi_i(\delta_i - \boldsymbol{\delta}^{\mathrm{T}}\Phi)\sigma_{\mathrm{e}}'(\phi) + \left[\delta_i\delta_{ij} - \delta_j\phi_i - \frac{\phi_i}{\phi}(\delta_i - \boldsymbol{\delta}^{\mathrm{T}}\Phi)\right]\sigma_{\mathrm{e}}(\phi)\right\}, \quad 1\leqslant i,j\leqslant N, \tag{2.31}$$

and we use the standard notation $\delta_{ij} = 1$ if $i = j$ and $\delta_{ij} = 0$ otherwise. For batch settling of a suspension in a closed column of height L, Eq. (2.30) is equipped with the initial condition

$$\Phi(z,0) = \Phi^0(z), \quad 0 < z < L, \quad \Phi^0(z) \in \mathscr{D}_{\phi_{\max}} \tag{2.32}$$

and the zero-flux boundary conditions

$$\mathbf{f}^{\mathrm{M}}(\Phi) - \mathbf{A}(\Phi)\frac{\partial \Phi}{\partial z} = 0 \quad \text{for } z = 0 \text{ and } z = L. \tag{2.33}$$

2.7. Batch centrifugation in a tube or basket centrifuge

We consider a moderate angular velocity ω for which both gravitational and Coriolis effects can be neglected, as discussed above. Then we may consider solutions that depend on the radius r as the unique space variable. Moreover, we introduce a parameter σ taking the value $\sigma = 0$ for a rotating tube and $\sigma = 1$ for a rotating basket centrifuge. In both cases it follows again that $q = 0$, and the system of equations that remains to be solved is

$$\frac{\partial \Phi}{\partial t} + \frac{1}{r^\sigma}\frac{\partial}{\partial r}\left(-\frac{\omega^2}{g}r^{1+\sigma}\mathbf{f}^{\mathrm{M}}(\Phi)\right) = \frac{1}{r^\sigma}\frac{\partial}{\partial r}\left(r^\sigma \mathbf{A}(\Phi)\frac{\partial \Phi}{\partial r}\right). \tag{2.34}$$

We assume that the radius r varies between an inner radius $R_{\mathrm{i}} > 0$ and an outer radius $R_{\mathrm{o}} > R_{\mathrm{i}}$. We then obtain the boundary conditions (analogous to (2.33))

$$-\frac{\omega^2 r_{\mathrm{b}}}{g}\mathbf{f}^{\mathrm{M}}(\Phi) - \mathbf{A}(\Phi)\frac{\partial \Phi}{\partial r}\bigg|_{r=r_{\mathrm{b}}} = 0 \quad \text{for } r_{\mathrm{b}} \in \{R_{\mathrm{o}}, R_{\mathrm{i}}\}, \tag{2.35}$$

and the initial condition

$$\Phi(r,0) = \Phi^0(r), \quad R_{\mathrm{i}} < r < R_{\mathrm{o}}, \quad \Phi^0(r) \in \mathscr{D}_{\phi_{\max}}. \tag{2.36}$$

3. Type analysis

We now summarize the main aspects of the type analysis by looking first at the gravity system (2.30). To this end, we consider first a suspension of rigid spheres forming incompressible sediments, such that $\sigma_{\mathrm{e}} \equiv 0$. Under this assumption, (2.30) reduces to the system of first-order conservation laws

$$\frac{\partial \Phi}{\partial t} + \frac{\partial \mathbf{f}^{\mathrm{M}}(\Phi)}{\partial z} = 0. \tag{3.1}$$

It is well known that solutions of (3.1) are discontinuous in general, and that the propagation speed $\sigma_i(\Phi^+, \Phi^-)$ of a discontinuity in the concentration field ϕ_i separating the states Φ^+ and Φ^- is given by the Rankine–Hugoniot condition

$$\sigma_i = \frac{f_i^{\mathrm{M}}(\Phi^+) - f_i^{\mathrm{M}}(\Phi^-)}{\phi_i^+ - \phi_i^-}, \quad i = 1, \ldots, N.$$

We recall that a system of conservation laws (3.1) is called *hyperbolic* if the eigenvalues of the Jacobian $\mathscr{J}_{\mathbf{f}^{\mathrm{M}}}(\Phi) := (\partial f_i/\partial \phi_k)_{1 \leqslant i,k \leqslant N}$ are real, and *strictly hyperbolic* if these are moreover pairwise distinct. For $N = 2$, a system with a pair of complex conjugate eigenvalues is called *elliptic*. Some of the flux-density vectors $\mathbf{f}(\Phi)$ proposed in the literature cause the system (3.1) to be non-hyperbolic. In the special case $N = 2$, this means that the system is of mixed hyperbolic–elliptic type. The loss of hyperbolicity depends on the size and density parameters, and the type is *mixed* if for given sizes and densities, the system is non-hyperbolic (or elliptic) for $\Phi \in E \subset \mathscr{D}^0_{\phi_{\max}}$, where

$$\mathscr{D}^0_{\phi_{\max}} := \{\Phi \in \mathbb{R}^N : \phi_1 > 0, \ldots, \phi_N > 0,\ \phi = \phi_1 + \cdots + \phi_N < \phi_{\max}\},$$

where it is assumed that $V(\phi) = 0$ for $\phi \geqslant \phi_{\max}$, and $\mathscr{D}^0_{\phi_{\max}} \setminus E$ is non-empty.

The ellipticity criterion is equivalent to the criterion for the occurrence of instabilities like blobs and viscous fingering (Fig. 2) introduced by Batchelor and Janse van Rensburg (1986), see Weiland et al. (1984) for pertinent experimental findings. By a perturbation analysis, Bürger et al. (2002) show that loss of hyperbolicity, that is the occurrence of at least one pair of complex conjugate eigenvalues of $\mathscr{J}_{\mathbf{f}}(\Phi)$ for vectors Φ belonging to some non-empty subset $E \subset \mathscr{D}_{\phi_{\max}}$, provides an instability criterion for polydisperse suspensions of *arbitrary* numbers of species N. For $N = 3$, this criterion can still be evaluated conveniently by calculating the discriminant

$$I_3(\Phi) := 4s^3 - s^2r^2 + 27t^2 + 4r^3t - 18rst$$

of the (signed) characteristic polynomial

$$p_3(\lambda; \Phi) := -\det(\mathscr{J}_{\mathbf{f}}(\Phi) - \lambda \mathbf{I}) = \lambda^3 + r\lambda^2 + s\lambda + t,$$

where the coefficients $r = r(\Phi)$, $s = s(\Phi)$ and $t = t(\Phi)$ are given by

$$r := -\mathrm{tr}\,\mathscr{J}_{\mathbf{f}} = -\frac{\partial f_1}{\partial \phi_1} - \frac{\partial f_2}{\partial \phi_2} - \frac{\partial f_3}{\partial \phi_3}, \quad t := -\det \mathscr{J}_{\mathbf{f}},$$

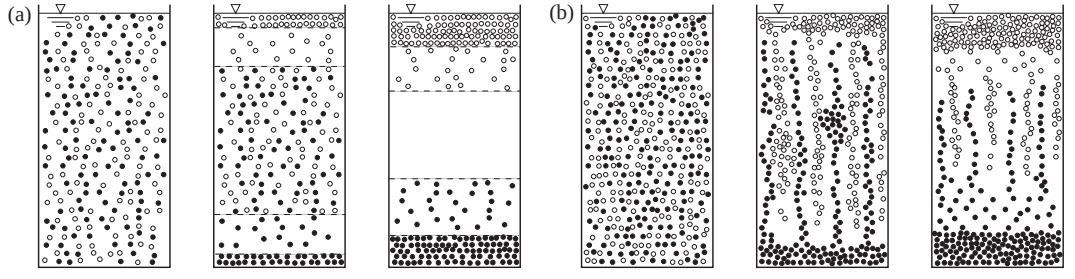

Fig. 2. Separation of a bidisperse suspension of heavy ($\varrho_1 > \varrho_f$; ●) and buoyant ($\varrho_2 < \varrho_f$; ○) particles: (a) stable demixing with horizontal interfaces at low initial concentrations, (b) unstable separation with formation of 'fingers' and 'blobs' at higher concentrations.

$$s := -\frac{\partial f_1}{\partial \phi_3}\frac{\partial f_3}{\partial \phi_1} - \frac{\partial f_1}{\partial \phi_2}\frac{\partial f_2}{\partial \phi_1} - \frac{\partial f_2}{\partial \phi_3}\frac{\partial f_3}{\partial \phi_2} + \frac{\partial f_1}{\partial \phi_1}\frac{\partial f_2}{\partial \phi_2} + \frac{\partial f_1}{\partial \phi_1}\frac{\partial f_3}{\partial \phi_3} + \frac{\partial f_2}{\partial \phi_2}\frac{\partial f_3}{\partial \phi_3}.$$

The model equations are unstable at $\Phi \in \mathscr{D}_{\phi_{\max}}$, that is, they are non-hyperbolic, when the equation $p_3(\lambda;\Phi) = 0$ has a pair of complex conjugate solutions, which occurs if and only if $I_3 > 0$. This also handles the bidisperse case. In fact, setting $I_2 := -I_3(\phi_1, \phi_2, 0)$, we get $I_2 = -s^2(r^2 - 4s)/108$; and Batchelor and Janse van Rensburg's (1986) well-known instability criterion for bidisperse suspensions just states that instabilities occur if

$$r^2 - 4s = \left(\frac{\partial f_1}{\partial \phi_1} + \frac{\partial f_2}{\partial \phi_2}\right)^2 - 4\left(\frac{\partial f_1}{\partial \phi_1}\frac{\partial f_2}{\partial \phi_2} - \frac{\partial f_1}{\partial \phi_2}\frac{\partial f_2}{\partial \phi_1}\right) = \left(\frac{\partial f_1}{\partial \phi_1} - \frac{\partial f_2}{\partial \phi_2}\right)^2 + 4\frac{\partial f_1}{\partial \phi_2}\frac{\partial f_2}{\partial \phi_1} < 0.$$

Bürger et al. (2002) determine instability regions (evaluating numerically I_3) for three different choices of $\mathbf{f}(\Phi)$. For the MLB model and a suspension with two particle species differing in size only, such instability regions are shown in Fig. 3. One of the predictions of the diagrams of Fig. 3 is that if we consider a bidisperse suspension with initial concentrations (ϕ_1^0, ϕ_2^0) chosen from the interior of the instability region, then this suspension will separate unstably according to Fig. 2(b); otherwise, it will separate stably under formation of stable horizontal interfaces as in Fig. 2(a). Observe that the instability regions for γ close to one in the left diagram of Fig. 3 are located near the line $\phi = 1$. This means that for bidisperse suspensions of equal-sized heavy particles that differ only slightly in density, hyperbolicity can be recovered by cutting the hindered settling factor $V(\phi)$ at a suitable maximum concentration $\phi_{\max}$, such that the instability region is contained in $\mathscr{D}_1 \setminus \mathscr{D}_{\phi_{\max}}$ and thus is irrelevant for computations. For the Richardson–Zaki hindered settling factor (2.22) this means that one utilizes

$$V(\phi) = \begin{cases} (1-\phi)^{n-2}, & n > 2 \quad \text{for } 0 < \phi < \phi_{\max}, \\ 0 & \text{otherwise} \end{cases}$$

instead of (2.22). For example, in the case $\gamma = 0.3$ we may choose $\phi_{\max} = 0.7$ (or, of course, any smaller value).

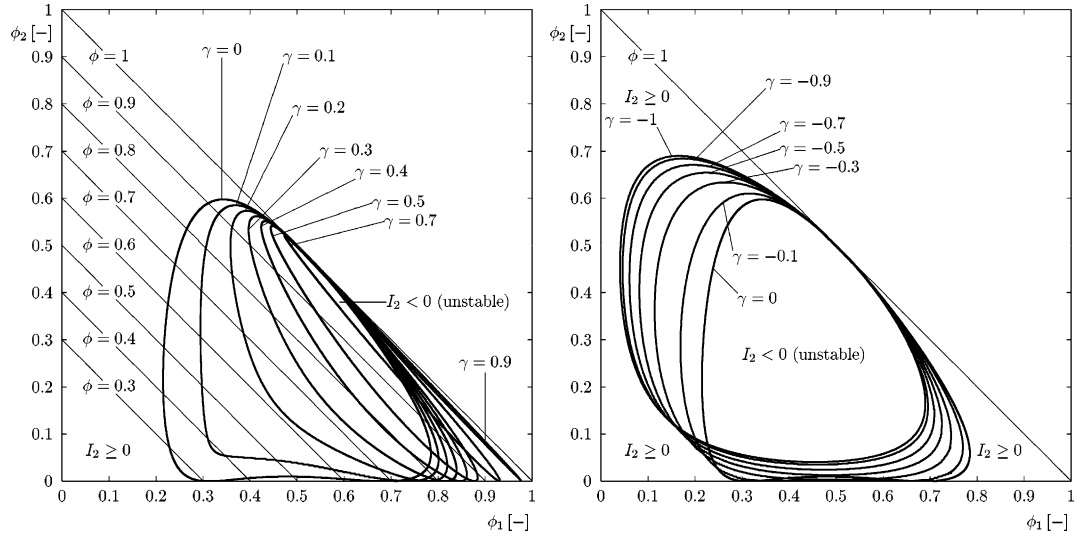

Fig. 3. Instability regions of the MLB model for $N = 2$ with $V(\phi) = (1-\phi)^{2.65}$ and particles of the same size ($d_1 = d_2$) and indicated relative density ratios $\gamma := \bar{\varrho}_2/\bar{\varrho}_1$ (Bürger et al., 2002). The left and right diagrams correspond to bidisperse suspensions with two heavy and one heavy and one buoyant (creaming) particle species, and include the instability region for the common limiting case $\gamma = 0$.

Fig. 6 of Batchelor and Janse van Rensburg (1986) shows good agreement of experimentally observed instability regions (in the phase plane) with those obtained algebraically, as those shown in our Fig. 3.

An interesting subcase is that of polydisperse suspensions of equal-density particles, usually made from the same material, which differ only in size. Biesheuvel et al. (2001) consider bidisperse ($N = 2$) suspensions with particles differing in both size and density and determine instability regions for the MLB model and the (more involved) model by Patwardhan and Tien (1985). They provide a long list of references (not repeated here) of experimental studies which indicate that instability phenomena have never been observed with equal-density (i.e., $\varrho_1 = \cdots = \varrho_N$) polydisperse suspensions. Biesheuvel et al. (2001) conjecture (but are not able to prove) that this equal-density case always leads to stable separations. In our mathematical terminology, this means that the equations should always be hyperbolic, but Biesheuvel et al. (2001) do not appeal to the instability criterion as a property of the type of the model equations. For $N = 2$ and the case $\varrho_1 = \varrho_2$, Bürger et al. (2002) prove algebraically by evaluating I_2 with the partial derivatives $\partial f_i^{\mathrm{M}}(\Phi)/\partial\phi_k$, $i,k = 1,2$ generated from the MLB model, that this conjecture is indeed true, which means that in this special case the model equations are always hyperbolic. More recently, Berres et al. (2003a) extend this result to any number of particle species N. In fact, by evaluating the characteristic polynomial $p(\lambda;\Phi) = \det(\mathscr{J}_{\mathbf{f}^{\mathrm{M}}}(\Phi) - \lambda\mathbf{I})$ they prove that for equal-density particles ($\bar{\varrho} = \cdots = \bar{\varrho}_N = \varrho_{\mathrm{s}} - \varrho_{\mathrm{f}}$), arbitrary N and particle size distributions, the system (3.1) is strictly hyperbolic for all $\Phi \in \mathscr{D}$ with $\phi_1 > 0, \ldots, \phi_N > 0$ and $\phi < 1$ if the flux vector (2.25) is chosen. The results of the type analysis of the first-order system (3.1) are also reported in Bürger (2002a,b).

Next, we include the compression effect and consider the full equations (2.30). We recall here that the assumption $\sigma_{\mathrm{e}} = \sigma_{\mathrm{e}}(\phi)$ used in the construction of the matrix $\mathbf{A}(\Phi)$ is very unlikely to hold if the particles differ in density, that is, differ in material, so we consider the compression effect given by the terms on the right-hand part of (2.30) only in combination with equal-density particles.

In view of the generic assumptions on $\sigma_{\mathrm{e}}(\phi)$ (2.8), we can read off from (2.31) that the system (2.30) is degenerate, i.e. changes from second to first order, since $\mathbf{A}(\Phi) = 0$ wherever $\phi \leqslant \phi_{\mathrm{c}}$, and we recall that for $\phi \leqslant \phi_{\mathrm{c}}$ and equal-density particles, the system (2.30) is strictly hyperbolic. Moreover, (2.30) has the non-obvious property of being parabolic for $\phi_{\mathrm{c}} < \phi < 1$, which means that $\mathbf{A}(\Phi)$ has N real, positive eigenvalues. This is proved by Berres et al. (2003a) by exploiting the similar properties of the characteristic polynomials of the Jacobian of the convective flux $\mathscr{J}_{\mathbf{f}}^{\mathrm{M}}(\Phi)$ and of the diffusion matrix $\mathbf{A}(\Phi)$. Furthermore, it turns out that the eigenvalues of $\mathbf{A}(\Phi)$ are pairwise distinct and bounded.

It can be easily checked that for a given vector $\Phi \in \mathscr{D}_{\max}$, the type of the 'centrifugal' system of equations (2.34) is the same as that of the analogous 'gravity' system (2.30) (with the same particle properties and model functions $V(\phi)$ and $\sigma_{\mathrm{e}}(\phi)$ chosen), and that the type does not depend on ω or r. To see this, we rewrite (2.34) in non-conservative form as

$$\frac{\partial\Phi}{\partial t} + \left(-\frac{\omega^2}{g} r \mathscr{J}_{\mathbf{f}^{\mathrm{M}}}(\Phi) - \frac{\sigma}{r}\mathbf{A}(\Phi) \right) \frac{\partial\Phi}{\partial r} = \frac{\partial}{\partial r}\left(\mathbf{A}(\Phi)\frac{\partial\Phi}{\partial r} \right) + \frac{\omega^2}{g}(1+\sigma)\mathbf{f}^{\mathrm{M}}(\Phi). \tag{3.2}$$

If Φ is chosen such that $\phi_{\mathrm{c}} < \phi < 1$, then the type of (3.2) is determined by the diffusion term, that is the first term on the right-hand part of (3.2). This term is identical to that appearing in (2.30), except for z being replaced by r. On the other hand, for $0 < \phi \leqslant \phi_{\mathrm{c}}$, (3.2) reduces to

$$\frac{\partial\Phi}{\partial t} - \frac{\omega^2}{g} r \mathscr{J}_{\mathbf{f}^{\mathrm{M}}}(\Phi)\frac{\partial\Phi}{\partial r} = \frac{\omega^2}{g}(1+\sigma)\mathbf{f}^{\mathrm{M}}(\Phi). \tag{3.3}$$

It is obvious that the relevant Jacobian of (3.3), which determines the type of these equations, is just that of the first-order 'gravity' equation (3.1), $\mathscr{J}_{\mathbf{f}}^{\mathrm{M}}(\Phi)$, multiplied by $-\omega^2 r/g$. Note that we consider $r \geqslant R_{\mathrm{i}} > 0$. Thus, (3.3) is hyperbolic if and only if (3.1) is.

Considering the full range $0 < \phi < \phi_{\max}$, we can in particular conclude that for equal-density spheres, both the 'gravity' system (2.30) and the 'centrifugal' system (2.34) provide examples of a strongly degenerate

parabolic–hyperbolic system of partial differential equations. It should, however, be mentioned that instability phenomena such as those depicted in Fig. 2 have not been recorded for centrifugal systems.

The type properties discussed in this section are not only theoretically interesting but are useful when it comes to numerical simulation. In fact, the properties of both matrices can be utilized to control the numerical diffusion of the numerical scheme by Kurganov and Tadmor (2000) applied to (2.30).

4. Numerical method

We consider the computational domain $Q_T := [R_\mathrm{i}, R_0] \times [0, T]$ and introduce a rectangular grid by setting $r_j := R_\mathrm{i} + j\Delta r$, where J is an even integer and $\Delta r := (R_\mathrm{o} - R_\mathrm{i})/J$ denotes the width of a half-cell. Moreover, let $t_n := n\Delta t$, $n = 0, 1, 2, \ldots, \mathscr{N}$, where $\Delta t := T/\mathscr{N}$, and $\mathscr{N}$ is an integer, and $\lambda := \Delta t/(2\Delta r)$. The (approximate) cell average of ϕ_i, $i = 1, \ldots, N$, with respect to the cell $[r_j, r_{j+2}]$, $j = 0, 2, 4, \ldots, J-2$, at time t_n is denoted by $\bar{\phi}^n_{i,j}$, $j = 1, 3, \ldots, J-1$, and we define the approximate cell-average vector $\bar{\boldsymbol{\Phi}}^n_j := (\bar{\phi}^n_{1,j}, \ldots, \bar{\phi}^n_{N,j})^\mathrm{T}$ for $j = 1, 3, \ldots, J-1$ and $n = 0, 1, \ldots, \mathscr{N}$.

To outline the scheme, assume that at time $z = t_n$, $n = 0, 1, \ldots, \mathscr{N}-1$, the vector $\bar{\boldsymbol{\Phi}}^n_j$ has either been calculated from the previous time step (for $n \geqslant 1$) or is given by the discretization of the initial condition,

$$\bar{\phi}^0_{i,j} := \frac{1}{2\Delta r}\int_{r_{j-1}}^{r_{j+1}} \phi^0_i(s)\,\mathrm{d}s, \quad j = 1, 3, \ldots, J-1,\ i = 1, \ldots, N.$$

For the interior cells, we obtain the explicit update formula

$$\bar{\boldsymbol{\Phi}}^{n+1}_j = \bar{\boldsymbol{\Phi}}^n_j + \frac{\omega^2\lambda}{r^\sigma_j g}\left(r^{1+\sigma}_{j+1}\mathbf{h}^n_{j+1} - r^{1+\sigma}_{j-1}\mathbf{h}^n_{j-1}\right) + \frac{\lambda}{r^\sigma_j}\left(r^\sigma_{j+1}\mathbf{p}^n_{j+1} - r^\sigma_{j-1}\mathbf{p}^n_{j-1}\right), \quad j = 3, 5, \ldots, J-3,$$
$$n = 0, 1, \ldots, \mathscr{N}-1. \tag{4.1}$$

Eq. (4.1) is the discrete analogue of the 'centrifugal' field equation (2.34), where $\mathbf{h}^n_{j\pm1}$ and $\mathbf{p}^n_{j\pm1}$ are approximations of the 'hyperbolic' and 'parabolic' fluxes $\mathbf{f}^\mathrm{M}$ and $\mathbf{a}$, respectively, through the boundaries of the cell $[r_{j-1}, r_{j+1}]$ at time t_n. The detailed computation of the numerical fluxes follows precisely that of the gravitational case described in detail in Section 6.2 of Berres et al. (2003a) (with the obvious modification of replacing 'z' by 'r'), and is therefore not repeated here.

While the interior scheme (4.1) approximates the field equation (2.34), the corresponding boundary conditions (2.35) prescribed at $r = R_\mathrm{i}$ and $r = R_\mathrm{o}$ are discretized by setting

$$-\frac{\omega^2 R_\mathrm{i}}{g}\mathbf{h}^n_0 - \mathbf{p}^n_0 = 0, \quad -\frac{\omega^2 R_\mathrm{o}}{g}\mathbf{h}^n_J - \mathbf{p}^n_J = 0, \qquad n = 0, 1, \ldots, \mathscr{N}-1. \tag{4.2}$$

Inserting this into (4.1), where we set $j = 1$ and $j = -1$, we obtain the following update formulas for the boundary cells (boundary scheme):

$$\bar{\boldsymbol{\Phi}}^{n+1}_1 = \bar{\boldsymbol{\Phi}}^n_1 + \frac{\omega^2\lambda}{r^\sigma_1 g}r^{1+\sigma}_2\mathbf{h}^n_2 + \frac{\lambda}{r^\sigma_1}r^\sigma_2\mathbf{p}^n_2, \quad n = 0, 1, \ldots, \mathscr{N}-1, \tag{4.3}$$

$$\bar{\boldsymbol{\Phi}}^{n+1}_{J-1} = \bar{\boldsymbol{\Phi}}^n_{J-1} - \frac{\omega^2\lambda}{r^\sigma_{J-1} g}r^{1+\sigma}_{J-2}\mathbf{h}^n_{J-2} - \frac{\lambda}{r^\sigma_{J-1}}r^\sigma_{J-2}\mathbf{p}^n_{J-1}, \quad n = 0, 1, \ldots, \mathscr{N}-1. \tag{4.4}$$

A necessary condition for the scheme to converge is that the CFL stability condition is satisfied, which limits the mesh size ratio $\lambda = \Delta t/\Delta r$ for the explicit scheme considered here. The extension of the CFL condition stated by Kurganov and Tadmor to the present strongly degenerate parabolic–hyperbolic system reads

$$\frac{\omega^2}{g}\frac{R_o}{R_i}\frac{\Delta t}{\Delta r}\max_{\mathscr{D}_{\phi_{\max}}}\rho(\mathscr{J}_{\mathbf{f}}(\Phi))+\frac{\Delta t}{2\Delta r^2}\max_{\mathscr{D}_{\phi_{\max}}}\rho(\mathbf{A}(\Phi))\leqslant\frac{1}{4}, \tag{4.5}$$

where $\rho(\cdot)$ denotes the spectral radius function.

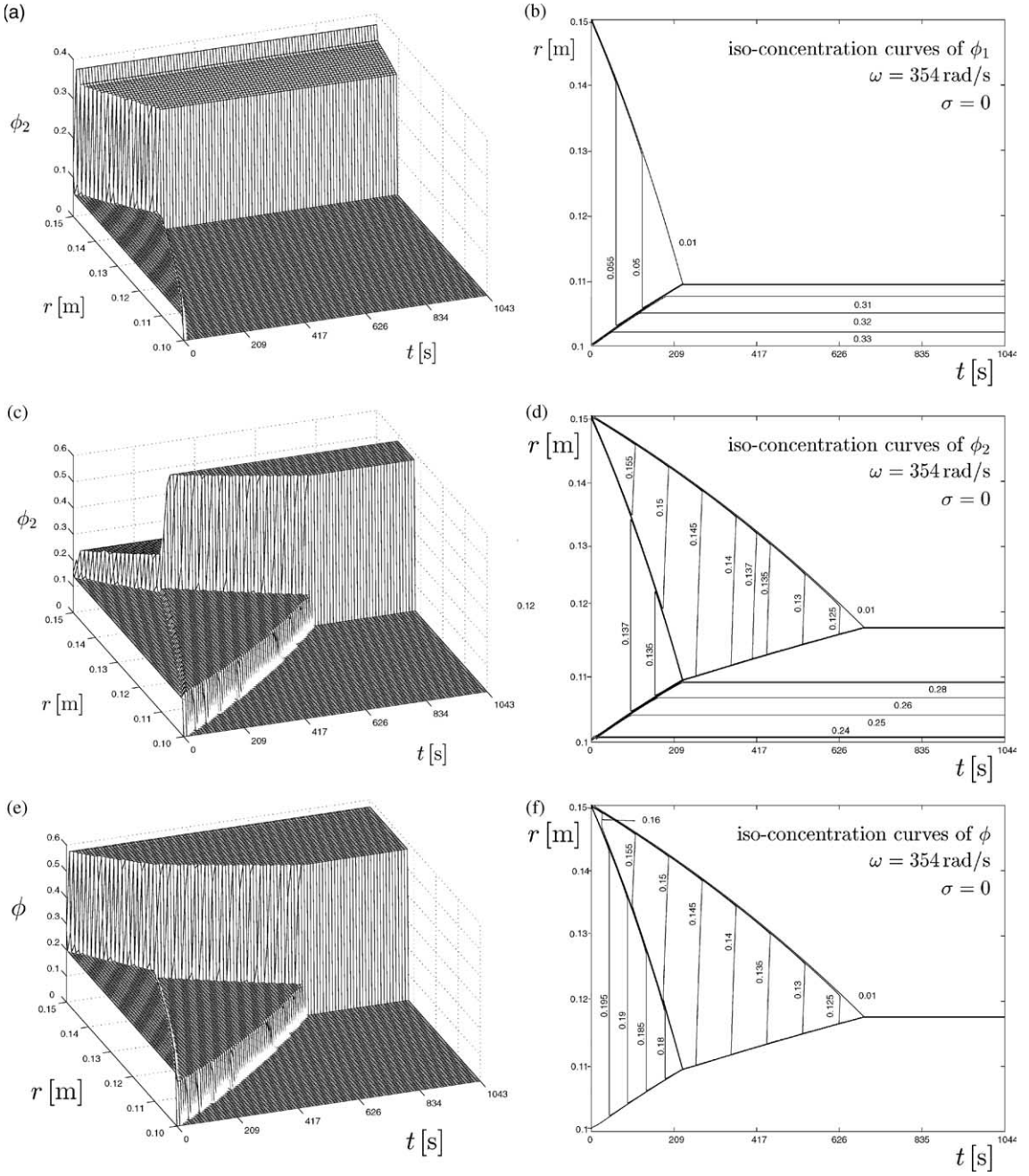

Fig. 4. Numerical simulation of batch centrifugation of a bidisperse suspension with particles differing in size and density.

5. Numerical examples

5.1. Centrifugation of a bidisperse suspension of rigid particles

Biesheuvel and Verweij (2000) consider batch centrifugal sedimentation as a procedure for manufacturing functionally graded materials. They consider a bidisperse suspension of zirconia (ZrO_2) and alumina (Al_2O_3) particles, which we identify with Species 1 and 2, respectively, dispersed in water, and use experimental information by Chang et al. (1991). According to Table IV of Biesheuvel and Verweij (2000), the particles have the parameters $d_1 = 3.0 \times 10^{-7}$ m, $d_2 = 2.0 \times 10^{-7}$ m, $\varrho_1 = 6050$ kg/m^3, $\varrho_2 = 3940$ kg/m^3,

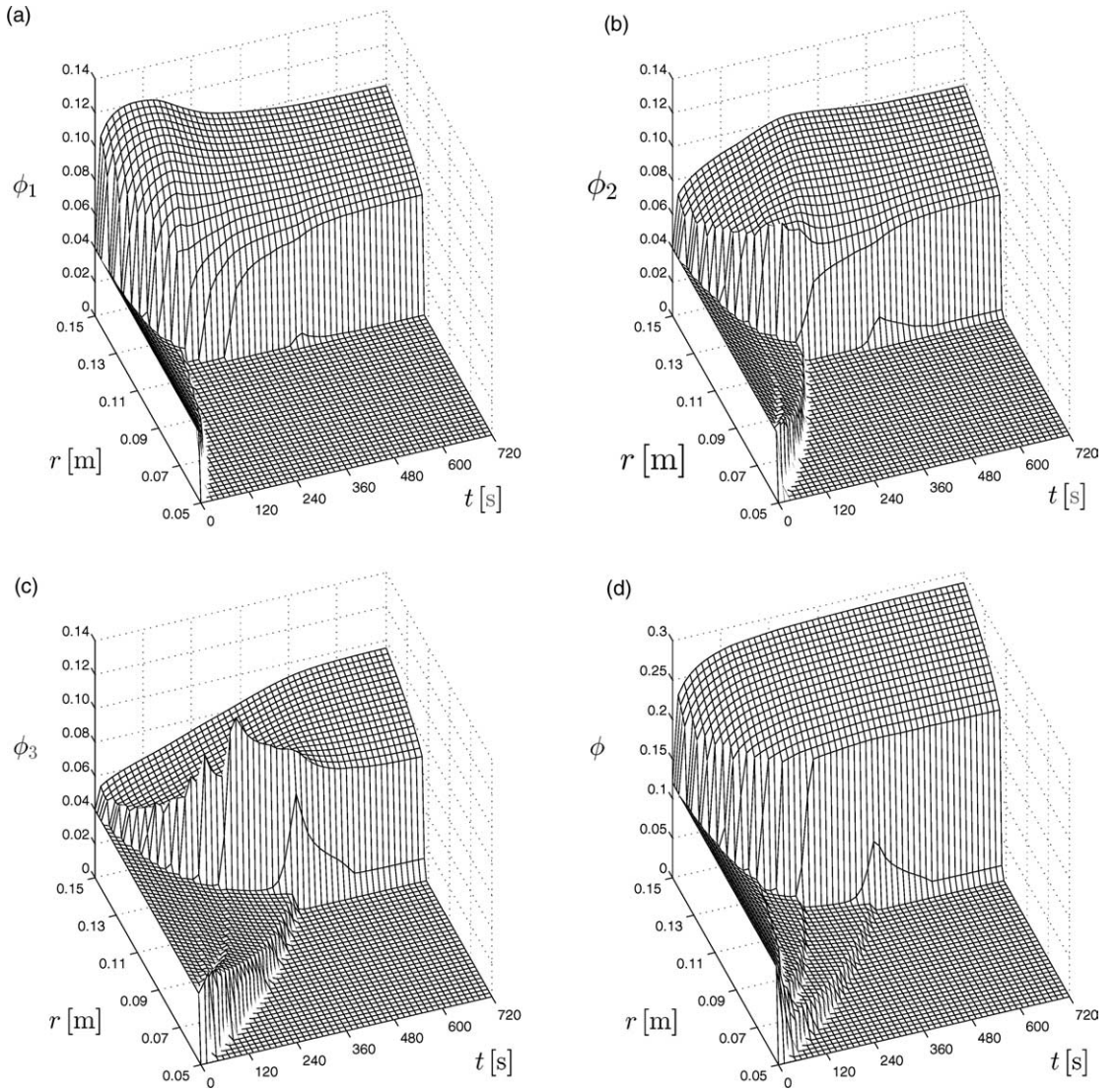

Fig. 5. Numerical simulation of the centrifugation of a tridisperse suspension forming compressible sediment in a basket centrifuge ($\sigma = 1$) at $\omega = \omega_1 = 25.573$ rad/s, showing (a–c) the concentrations of the individual species and (d) the cumulative concentration ϕ.

while those of the liquid are, as before, $\varrho_f = 1000$ kg/m^3 and $\mu_f = 10^{-3}$ Pa s. The initial concentration of the mixture considered is $\phi_1^0 = 0.06$ and $\phi_2^0 = 0.14$, and a tube centrifuge ($\sigma = 0$) is considered with the radii $R_i = 0.1016$ m and $R_o = 0.1524$ m. The centrifuge is operated at the scalar angular velocity $\omega = 354$ rad/s, which produces a centrifugal acceleration of $\omega^2 R = 1946.8g$ at the outer radius. Biesheuvel and Verweij (2000) indicate that the hindered settling function (2.22) with $n = 4.65$ is appropriate, and consider a 'packing factor' of 0.573, which we consider as a maximum concentration ϕ_{max} at which the hindered settling factor $V(\phi)$ is cut.

We verified by evaluating the discriminant I_2 numerically at a sufficiently dense set of points $(\phi_1, \phi_2) \in \mathscr{D}^0_{0.573}$ that the MLB model with these parameters is indeed strictly hyperbolic, although the system considered here involves particles of different sizes *and* different densities, for which this property usually does not hold. The numerical simulations were made by considering $R_i = 0.1$ m, $R_o = 0.15$ m, $J = 1000$ and $\lambda = 1$ s/m. The numerical result is shown in Fig. 4 as three-dimensional plots of the concentrations as functions of radius r and time t and as settling plots. The solution shows that the bulk

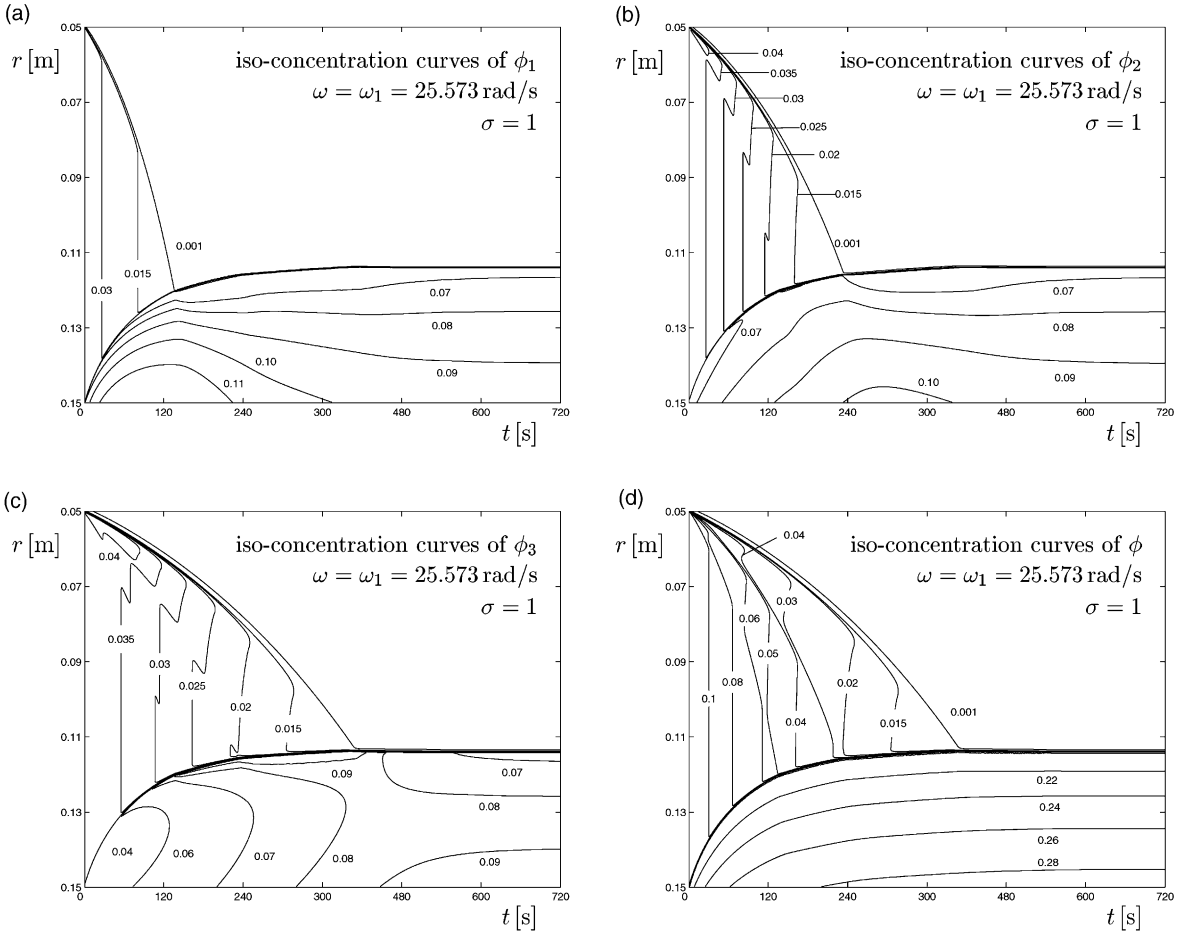

Fig. 6. Numerical simulation of the centrifugation of a tridisperse suspension forming compressible sediment in a basket centrifuge at $\omega = \omega_1 = 25.573$ rad/s, showing (a–c) iso-concentration lines of the individual species and (d) of the cumulative concentration ϕ. These plots correspond to the results shown in Fig. 5.

suspension, in which the concentration of both species decreases with time, is separated from the clear supernatant liquid by two curved concentration discontinuities, which form a sector in which the suspension consists of the smaller particles only. Fig. 4(d) shows that the concentration ϕ_2 of the smaller species in this sector is larger than in the bulk suspension zone underneath, and for small times even larger than the initial concentration. This 'enrichment' of the smaller particles also appears in simulations of the gravity settling case (Bürger et al., 2001; Xue and Sun, 2003), was noted first by Smith (1966), and is therefore sometimes called Smith effect.

The sediments are assumed here to be incompressible, and turn out to be composed of two layers: an outer layer in which both particles are present at slightly varying concentrations, which accurately add up to the maximum concentration 0.573, and an inner layer where only the second (smaller) species is present, and also assumes the maximum concentration.

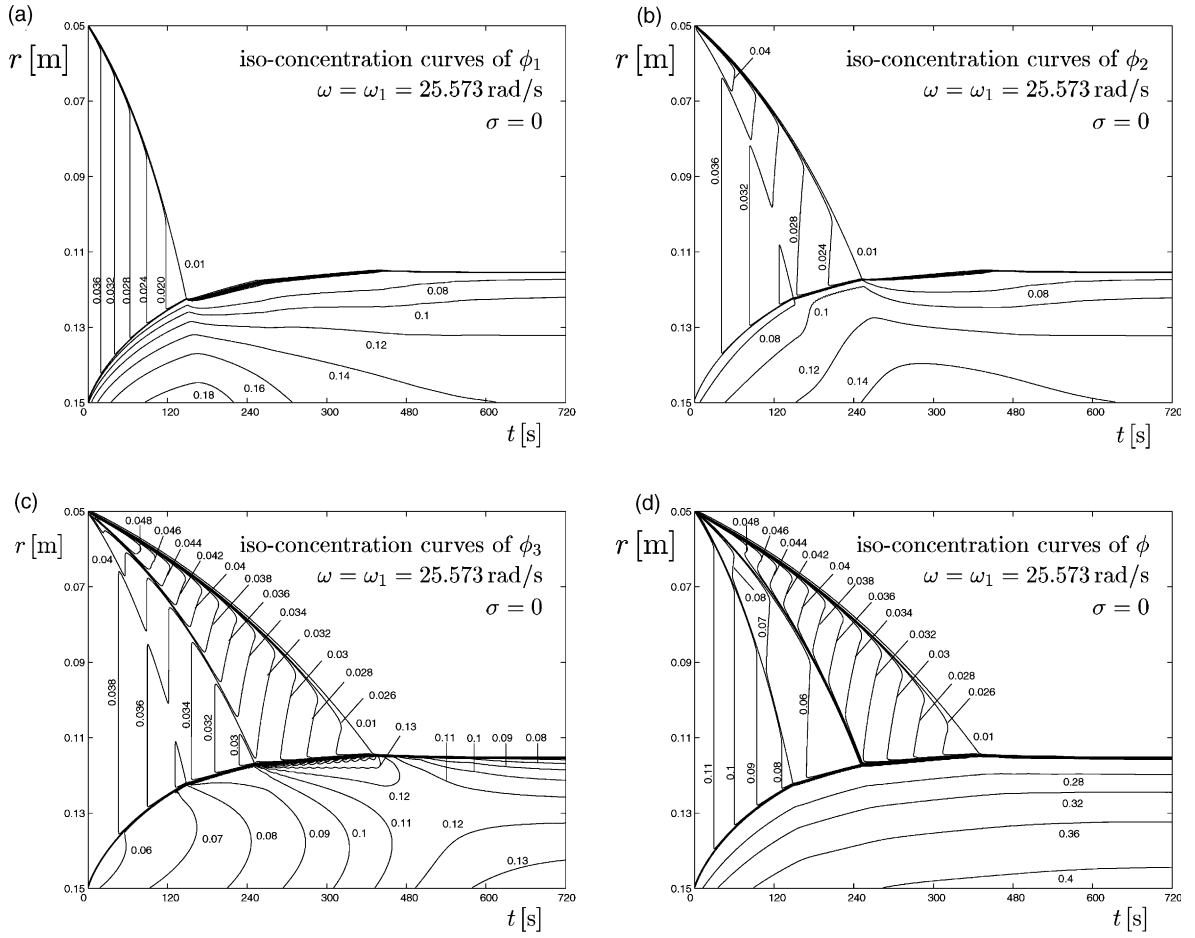

Fig. 7. Numerical simulation of the centrifugation of a tridisperse suspension forming compressible sediment in a tube centrifuge ($\sigma = 0$) at $\omega = \omega_1 = 25.573$ rad/s, showing (a–c) iso-concentration lines of the individual species and (d) of the cumulative concentration ϕ.

5.2. Centrifugation of a tridisperse suspension forming compressible sediments

We consider a tridisperse ($N = 3$) suspension forming compressible sediments. This physical properties of the mixture are the same as in Berres et al. (2003a), and are given by the model function (2.9) for $\sigma_e(\phi)$ with the parameters $\sigma_0 = 180$ Pa, $\phi_c = 0.2$ and $k = 6$, and by the hindered settling factor (2.22) with $n = 4.7$. The remaining parameters are $\mu_f = 10^{-3}$ Pa s, $d_1 = 1.19 \times 10^{-5}$ m, $d_2 = \sqrt{0.5}d_1$, $d_3 = 0.5d_1$ (such that $\boldsymbol{\delta} = (1, 0.5, 0.25)^T$), $\bar{\varrho}_s = 1800$ kg/m^3 and $g = 9.81$ m/s^2. We consider here both a tube ($\sigma = 0$) and a basket ($\sigma = 1$) centrifuge, where the inner and outer radii are chosen as $R_i = 0.05$ m and $R_o = 0.15$ m, such that the effective sedimenting space is $R_o - R_i = 0.1$ m. The angular velocity is first chosen as $\omega_1 = 25.573$ rad/s, such that $\omega^2 R_o = 10g$. To study the effect of increase of the radial velocity on the composition of the sediment, we consider in addition the same centrifuge as a basket centrifuge ($\sigma = 1$), operated at the angular velocities $\omega_2 = \sqrt{10}\omega_1$ and $\omega_3 = 10\omega_1$, such that the centrifugal acceleration at the outer radius is increased twice by a factor of ten. In all cases, we choose the initial concentrations $\Phi^0 = (0.04, 0.04, 0.04)$, as in Berres et al. (2003a).

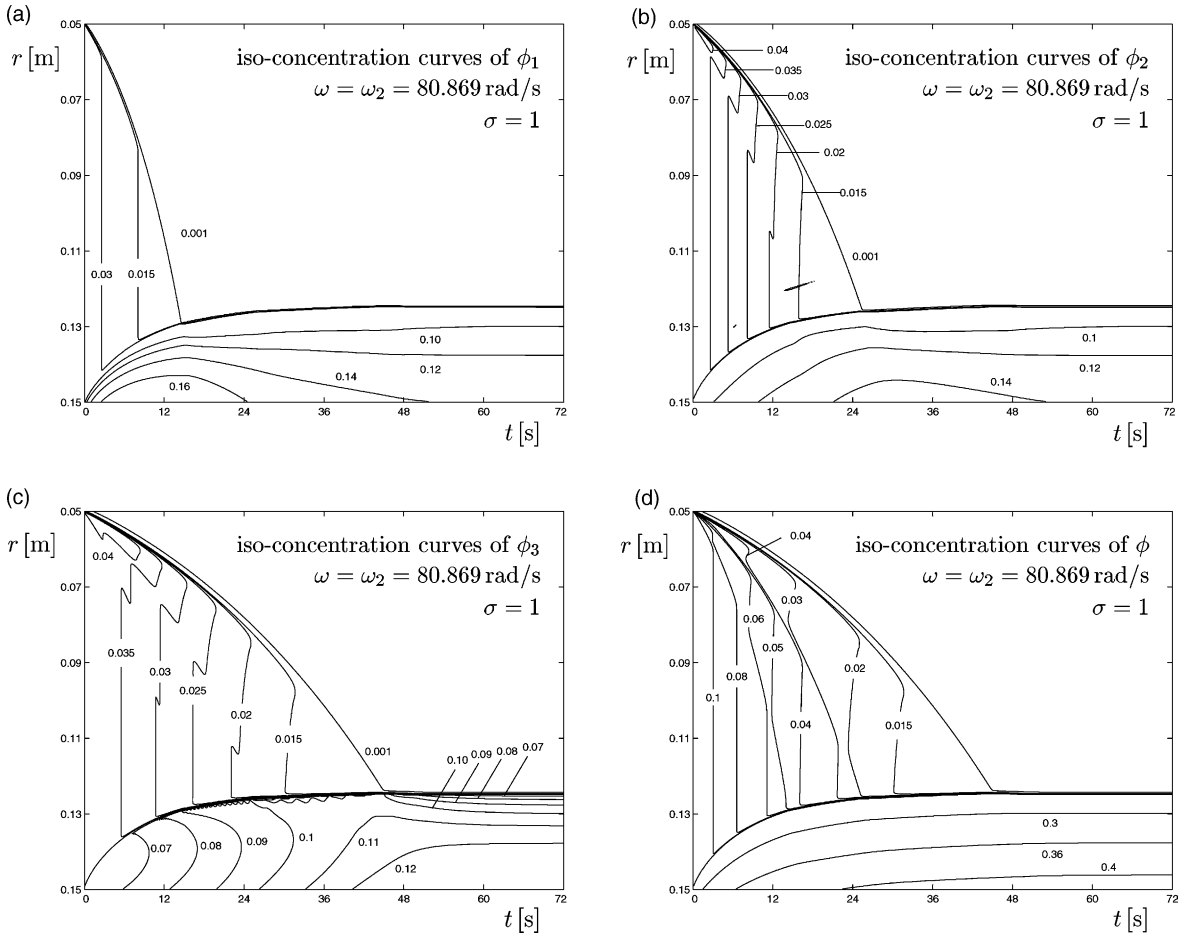

Fig. 8. Numerical simulation of the centrifugation of a tridisperse suspension forming compressible sediment in a basket centrifuge at $\omega = \omega_2 = 80.869$ rad/s, showing (a–c) iso-concentration lines of the individual species and (d) of the cumulative concentration ϕ.

In our simulations, we use the parameters $J = 1000$ and $\lambda = 8.0 \times 10^{-4}$ s/m, 8.0×10^{-5} s/m and 8.0×10^{-6} s/m for $\omega = \omega_1$, ω_2 and ω_3, respectively. Fig. 5 shows the numerical results for $\omega = \omega_1$ and $\sigma = 1$ as three-dimensional plots. Note that the grid used in the visual representation of these results is much coarser than the computational grid defined by the parameter Δr that was actually used for the computations. More accurate information is given by the plots of Fig. 6. We observe three curved discontinuities forming (from inner to outer positions) a clear supernatant liquid zone, a zone containing only the smallest species, a zone containing the smallest and intermediate species, and a zone in which all species are present. As for monodisperse suspensions (Anestis, 1981; Anestis and Schneider, 1983; Lueptow and Hübler, 1991; Bürger and Concha, 2001) and unlike the gravity case for polydisperse mixtures (Bürger et al., 2000a, 2001), concentrations are not constant in these zones but vary as functions of time. From the 'bottom', that is, from the outer wall of the basket centrifuge, the sediment is growing.

The plot showing the isolines of the cumulative solids concentration ϕ, Fig. 6(d) shows for t fixed that this concentration consistently increases from the suspension-sediment interface, where $\phi = \phi_c$, towards the outer wall, and that the maximum concentration reached at the outer wall increases in time, which becomes apparent by the successive appearance from the outer radius of the iso-concentration lines for $\phi = 0.22$,

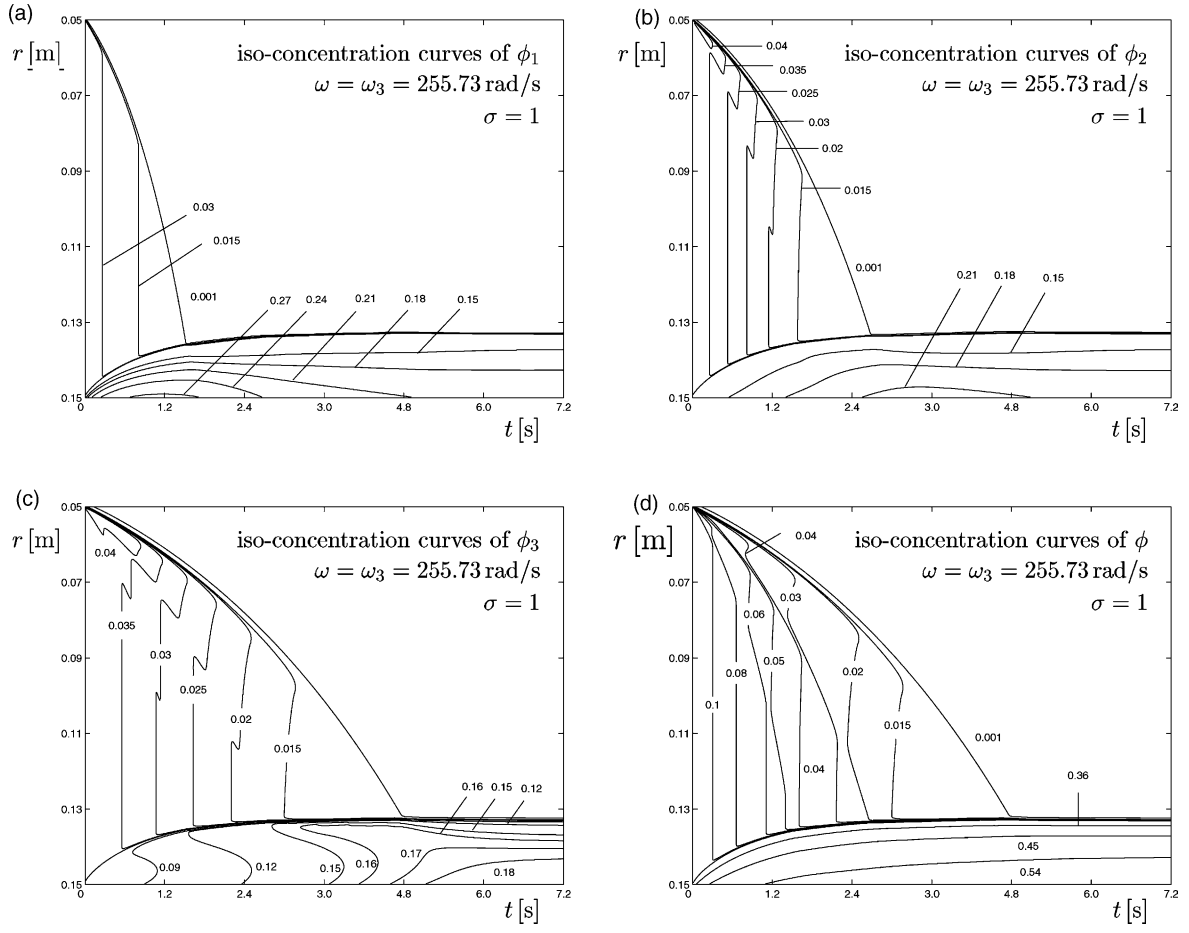

Fig. 9. Numerical simulation of the centrifugation of a tridisperse suspension forming compressible sediment in a basket centrifuge at $\omega = \omega_3 = 255.73$ rad/s, showing (a–c) iso-concentration lines of the individual species and (d) of the cumulative concentration ϕ.

0.24, 0.26 and 0.28. This behaviour is similar to the simulations shown by Bürger and Concha (2001) for monodisperse suspensions. The interesting parts of the solution are the iso-concentration lines of the concentrations ϕ_1 to ϕ_3 of the individual species. We observe in Fig. 6(a) and (b) that the concentrations of ϕ_1 and ϕ_2 increase near the bottom and then decrease again (as a function of time), and Figs. 5(d) and 6(d) indicate that the smallest species first form a thin layer with relatively high concentration at the top of the sediment before an equilibrium concentration is assumed. The numerical results indicate that the final concentration of each species at steady state is at a given height is one third of the cumulative solids concentration ϕ.

Fig. 7 refers to the same parameters as the example shown in Figs. 5 and 6 except that we here consider a rotating tube ($\sigma = 0$). The solution picture is very similar to that of Fig. 6, but the final concentrations attained at the outer wall are substantially higher than in the basket centrifuge case ($\sigma = 1$).

Figs. 8 and 9 again refer to the basket centrifuge ($\sigma = 1$) considered in Figs. 5 and 6, but at the increased radial velocities $\omega_2 = \sqrt{10}\omega_1$ and $\omega_3 = 10\omega_1$. Since the final time has been decreased by the factors 10 and 100 in Figs. 8 and 9, respectively, against that of Figs. 5 and 6, the solution pictures in the hindered settling zone (where $\phi \leqslant \phi_c$ look very much the same. However, Figs. 8 and 9 illustrate that increasing the angular velocity increases the concentrations in the sediment near the outer wall, and decreases the thickness of the sediment, as expected.

6. Discussion

The mathematical model presented herein allows for describing both the hindered settling and the consolidation of suspensions with particles of different sizes and densities by one system of field equations. Thus it is unnecessary to explicitly track the suspension-sediment interface. It has been shown that modern shock-capturing schemes for systems of conservation laws can be employed to simulate centrifugal sedimentation–consolidation processes of flocculated suspensions. In particular, these schemes accurately resolve concentration discontinuities, reproduce them at the right position, and also include discretizations of the diffusion terms describing sediment compressibility.

The present paper provides the common mathematical framework for recent analyses of gravity settling of polydisperse mixtures, including the authors' papers and, for example, Xue and Sun (2003), and of theoretical and experimental studies of centrifugal separation processes by Demeler et al. (1997); Biesheuvel et al. (1998), Biesheuvel and Verweij (2000), Lerche and Frömer (2001), Frömer and Lerche (2002) and Dück and Neeße (2002). However, in the centrifugal case some limitations of the applicability of the model herein have to be taken into account. One of them is the range of angular velocities discussed in Section 2.5. In fact, for very high values of ω the Coriolis effect will add significant azimuthal components to the particle phase velocities, and neglecting the Coriolis terms will then lead to under-predictions of the sedimentation time. In the monodisperse case, this effect has become visible in Fig. 7 of Bürger and Concha (2001). A related limitation becomes apparent for long tube centrifuges ($\sigma = 0$) and for basket centrifuges with compartment walls. In these cases the solid particles do not only settle onto the outer (radial) wall but also on the side walls of the tube or onto compartment walls. Obviously, it is then no longer sufficient to consider one space dimension. Extended analyses of mono- and bidisperse sedimentation including these cases are provided by Greenspan and Ungarish (1985), Schaflinger et al. (1986), Schaflinger (1987), Schaflinger and Stibi (1987) and Ungarish (1993, 1995, 2001). Let us mention that these treatments do not lead to easily solvable models describing the complete separation process. Moreover, most available experimental information the model could be compared with (i.e., which provides concentration profiles) is related to the gravity case, and there are currently only a few reliable records of sediment-suspension and suspension-supernate interfaces in the centrifugal case (Sambuichi et al., 1991; Eckert et al., 1996; Garrido et al., 2001).

Finally, we mention that the mathematical analysis of strongly degenerate parabolic–hyperbolic equations and systems such as (2.30) is an ongoing research topic with still many unresolved problems. In fact, only for the scalar case ($N = 1$) it is ensured that the sedimentation–consolidation model stated here is well-posed, which means that a solution exists, is unique, and continuously depends on the initial data, see Bürger and Karlsen (2001). For this case it is also possible to prove convergence of a numerical scheme. For $N \geqslant 2$, a closed well-posedness theory even for the special subcase (3.1) (let alone for the system (2.30)) is not available. Thus, rigorous convergence analyses of numerical schemes for such equations are feasible only in the scalar case. High-resolution shock-capturing schemes appear to be a powerful tool for the simulation of the dynamics of polydisperse suspensions, but it should clearly be pointed out that the recommendation of their use for the present class of problems is essentially based on numerical experimentation. It should also be mentioned that it is at present unclear under which conditions these schemes will produce meaningful solutions also in the first-order hyperbolic–elliptic (for $N = 2$) or non-hyperbolic mixed type cases discussed in Section 3.

Acknowledgement

We acknowledge support by the Collaborative Research Center (Sonderforschungsbereich) 404 at the University of Stuttgart.

References

Anestis, G., 1981. Eine eindimensionale Theorie der Sedimentation in Absetzbehältern veränderlichen Querschnitts und in Zentrifugen. Doctoral Thesis, Technical University of Vienna, Austria.

Anestis, G., Schneider, W., 1983. Application of the theory of kinematic waves to the centrifugation of suspensions. Ing.-Arch. 53, 399–407.

Arastoopour, H., Lin, S.C., Weil, S.A., 1982. Analysis of vertical pneumatic conveying of solids using multiphase flow models. AIChE J. 28, 467–473.

Batchelor, G.K., Janse van Rensburg, R.W., 1986. Structure formation in bidisperse sedimentation. J. Fluid Mech. 166, 379–407.

Berres, S., Bürger, R., Karlsen, K.H., Tory, E.M., 2003a. Strongly degenerate parabolic–hyperbolic systems modeling polydisperse sedimentation with compression. SIAM J. Appl. Math., to appear.

Berres, S., Bürger, R., Tory, E.M., 2003b. Mathematical model and numerical simulation of the liquid fluidization of polydisperse solid particle mixtures. Comput. Visual. Sci., to appear.

Biesheuvel, P.M., Nijmijer, A., Verweij, H., 1998. Theory of batchwise centrifugal casting. AIChE J. 44, 1914–1921.

Biesheuvel, P.M., Verweij, H., 2000. Calculation of the composition profile of a functionally graded material produced by centrifugal casting. J. Am. Ceram. Soc. 83, 743–749.

Biesheuvel, P.M., Verweij, H., Breedveld, V., 2001. Evaluation of instability criterion for bidisperse sedimentation. AIChE J. 47, 45–52.

Bürger, R., 2002a. Mathematical models for the sedimentation of polydisperse suspensions. In: Kittl, P., Díaz, G., Mook, D., Geer, J. (Eds.), Applied Mechanics in the Americas, vol. 9: Proceedings of the Seventh Pan American Congress of Applied Mechanics (PACAM VII), Temuco, Chile, 2–4 January 2002. American Academy of Mechanics/Universidad de La Frontera, Philadelphia, USA/Temuco, Chile, pp. 377–380.

Bürger, R., 2002b. On Mathematical Models for the Solid–Liquid Separation of Suspensions: Strongly Degenerate Convection–Diffusion Problems, Conservation Laws with Discontinuous Flux, and Systems of Conservation Laws. Habilitationsschrift, Faculty of Mathematics, University of Stuttgart.

Bürger, R., Concha, F., 2001. Settling velocities of particulate systems: 12. Batch centrifugation of flocculated suspensions. Int. J. Mineral Process. 63, 115–145.

Bürger, R., Concha, F., Fjelde, K.-K., Karlsen, K.H., 2000a. Numerical simulation of the settling of polydisperse suspensions of spheres. Powder Technol. 113, 30–54.

Bürger, R., Fjelde, K.-K., Höfler, K., Karlsen, K.H., 2001. Central difference solutions of the kinematic model of settling of polydisperse suspensions and three-dimensional particle-scale simulations. J. Eng. Math. 41, 167–187.

Bürger, R., Karlsen, K.H., 2001. A strongly degenerate convection–diffusion problem modeling centrifugation of flocculated suspensions. In: Freistühler, H., Warnecke, G. (Eds.), Hyperbolic Problems: Theory, Numerics, Applications. Eighth International Conference in Magdeburg, February/March 2000. Int. Ser. Numer. Math. 140, vol. I. Birkhäuser Verlag, Basel, pp. 207–216.

Bürger, R., Karlsen, K.H., Tory, E.M., Wendland, W.L., 2002. Model equations and instability regions for the sedimentation of polydisperse suspensions of spheres. Z. Angew. Math. Mech. 82, 699–722.

Bürger, R., Wendland, W.L., Concha, F., 2000b. Model equations for gravitational sedimentation–consolidation processes. Z. Angew. Math. Mech. 80, 79–92.

Chang, L.C., Velamakanni, B.V., Lange, F.F., Pearson, D.S., 1991. Centrifugal consolidation of Al_2O_3 and Al_2O_3/ZrO_2 composite slurries vs interparticle potentials: particle packing and mass segregation. J. Am. Ceram. Soc. 74, 2201–2204.

Concha, F., Bustos, M.C., Barrientos, A., 1996. Phenomenological theory of sedimentation. In: Tory, E. (Ed.), Sedimentation of Small Particles in a Viscous Fluid. Computational Mechanics Publications, Southampton, pp. 51–96.

Concha, F., Lee, C.H., Austin, L.G., 1992. Settling velocities of particulate systems: 8. Batch sedimentation of polydispersed suspensions of spheres. Int. J. Mineral Process. 35, 159–175.

Davis, R.H., Gecol, H., 1994. Hindered settling function with no empirical parameters for polydisperse suspensions. AICHE J. 40, 570–575.

Demeler, B., Saber, H., Hansen, J.C., 1997. Identification and interpretation of complexity in sedimentation velocity boundaries. Biophys. J. 72, 397–407.

Dück, J., Neeße, T., 2002. Experimentelle Untersuchungen und Modellbildung zur Sedimentation polydisperser Suspensionen. Lecture Notes, University of Erlangen-Nürnberg (in German).

Eckert, W.F., Masliyah, J.H., Gray, M.R., Fedorak, P.M., 1996. Prediction of sedimentation and consolidation of fine tails. AIChE J. 42, 960–972.

Fitt, A., 1996. Mixed systems of conservation laws in industrial mathematical modelling. Surv. Math. Ind. 6, 21–53.

Flotats, X., 1995. Mathematical modeling of polydisperse suspensions sedimentation. Hung. J. Ind. Chem. 23, 215–221.

Frömer, D., Lerche, D., 2002. An experimental approach to the study of the sedimentation of dispersed particles in a centrifugal field. Arch. Appl. Mech. 72, 85–95.

Garrido, P., Concha, F., Bürger, R., 2001. Application of the unified model of solid–liquid separation of flocculated suspensions to experimental results. In: da Luz, A.B., Soares, P.S.M., Torem, M.L., Trindade, R.B.E. (Eds.), Proceedings of the VI Southern Hemisphere Meeting on Mineral Technology, Rio de Janeiro, Brazil, May 27–31, 2001, vol. 1, CETEM/MCT, Rio de Janeiro, pp. 117–122.

Greenspan, H.P., Ungarish, M., 1985. On the centrifugal separation of a bulk mixture. Int. J. Multiphase Flow 11, 825–835.

Kurganov, A., Tadmor, E., 2000. New high-resolution central schemes for nonlinear conservation laws and convection–diffusion equations. J. Comput. Phys. 160, 241–282.

Lee, C.-H., 1989. Modeling of Batch Hindered Settling. PhD Thesis, College of Earth and Mineral Sciences, Pennsylvania State University, University Park, PA, USA.

Lerche, D., Frömer, D., 2001. Theoretical and experimental analysis of the sedimentation kinetics of concentrated red cell suspensions in a centrifugal field: Determination of the aggregation and deformation of RBC by flux density and viscosity functions. Biorheology 38, 259–262.

Lockett, M.J., Bassoon, K.S., 1979. Sedimentation of binary particle mixtures. Powder Technol. 24, 1–7.

Lueptow, R.M., Hübler, W., 1991. Sedimentation of a suspension in a centrifugal field. J. Biomech. Eng. 113, 485–491.

Masliyah, J.H., 1979. Hindered settling in a multiple-species particle system. Chem. Eng. Sci. 34, 1166–1168.

Massoudi, M., Rajagopal, R., Ekmann, J.M., Mathur, M.P., 1992. Remarks on the modeling of fluidized systems. AIChE J. 38, 471–472.

Nakamura, K., Capes, C.E., 1976. Vertical pneumatic conveying of binary particle mixtures. In: Keairns, D.L. (Ed.), Fluidization Technology, vol. 2. Hemisphere, Washington, pp. 159–184.

Nessyahu, H., Tadmor, E., 1990. Non-oscillatory central differencing for hyperbolic conservation laws. J. Comput. Phys. 87, 408–463.

Patwardhan, V.S., Tien, C., 1985. Sedimentation and liquid fluidization of solid particles of different sizes and densities. Chem. Eng. Sci. 40, 1051–1060.

Richardson, J.F., Zaki, W.N., 1954. Sedimentation and fluidization: Part I. Trans. Inst. Chem. Engrs. (London) 32, 35–53.

Sambuichi, M., Nakakura, H., Osasa, K., 1991. Zone settling of concentrated slurries in a centrifugal field. J. Chem. Eng. Japan 24, 489–494.

Schaflinger, U., 1987. Enhanced centrifugal separation with finite Rossby numbers in cylinders with compartment-walls. Chem. Eng. Sci. 42, 1197–1205.

Schaflinger, U., Stibi, H., 1987. On centrifugal separation of suspensions in cylindrical vessels. Acta Mech. 67, 163–181.

Schaflinger, U., Köppl, A., Filipczak, G., 1986. Sedimentation in cylindrical centrifuges with compartments. Ing.-Arch. 56, 321–331.

Shih, Y.T., Gidaspow, D., Wasan, D.T., 1986. Sedimentation of fine particles in nonaqueous media: Part I–Experimental, Part II–Modeling. Colloid. Surf. 21, 393–429.

Smith, T.N., 1966. The sedimentation of particles having a dispersion of sizes. Trans. Inst. Chem. Engrs. 44, T152–T157.
Stamatakis, K., Tien, C., 1992. Batch sedimentation calculations—the effect of compressible sediment. Powder Technol. 72, 227–240.
Tadmor, E., 1998. Approximate solutions of nonlinear conservation laws. In: Advanced Numerical Approximation of Nonlinear Hyperbolic Equations. In: Cockburn, B., Johnson, C., Shu, C.-W., Tadmor, E. (Eds.), Lecture Notes in Mathematics, vol. 1697. Springer-Verlag, Berlin, pp. 1–149.
Tiller, F.M., Leu, W.F., 1980. Basic data fitting in filtration. J. Chin. Inst. Chem. Engrs. 11, 61–70.
Ungarish, M., 1993. Hydrodynamics of Suspensions. Springer-Verlag, Berlin.
Ungarish, M., 1995. On the modeling and investigation of polydispersed rotating suspensions. Int. J. Multiphase Flow 21, 267–284.
Ungarish, M., 2001. On the separation of a suspension in a tube centrifuge. Int. J. Multiphase Flow 27, 1285–1291.
Weiland, R.H., Fessas, Y.P., Ramarao, B.V., 1984. On instabilities arising during sedimentation of two-component mixtures of solids. J. Fluid Mech. 142, 383–389.
Xue, B., Sun, Y., 2003. Modeling of sedimentation of polydisperse spherical beads with a broad size distribution. Chem. Eng. Sci. 58, 1531–1543.
Zeng, J., Lowe, D.R., 1992. A numerical model for sedimentation from highly-concentrated multi-sized suspensions. Math. Geol. 24, 393–415.